Since January 2020 Elsevier has created a COVID-19 resource centre with free information in English and Mandarin on the novel coronavirus COVID-19. The COVID-19 resource centre is hosted on Elsevier Connect, the company's public news and information website.

Elsevier hereby grants permission to make all its COVID-19-related research that is available on the COVID-19 resource centre - including this research content - immediately available in PubMed Central and other publicly funded repositories, such as the WHO COVID database with rights for unrestricted research re-use and analyses in any form or by any means with acknowledgement of the original source. These permissions are granted for free by Elsevier for as long as the COVID-19 resource centre remains active.

Applied Soft Computing Journal 97 (2020) 106800

Contents lists available at ScienceDirect

Applied Soft Computing Journal

journal homepage: www.elsevier.com/locate/asoc

Fuzzy Electromagnetism Optimization (FEMO) and its application in biomedical image segmentation

Shouvik Chakraborty *, Kalyani Mali

Department of Computer Science & Engineering, University of Kalyani, India

GRAPHICAL ABSTRACT

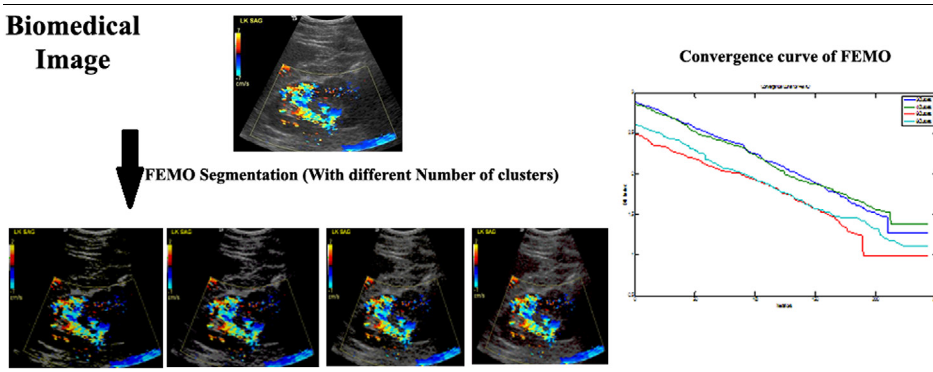

ARTICLE INFO

Article history:
Received 6 May 2020
Received in revised form 9 September 2020
Accepted 13 October 2020
Available online 16 October 2020

Keywords:
Biomedical image segmentation
Evolutionary algorithms
Fuzzy C-means clustering
Electromagnetism-like optimization
FEMO

ABSTRACT

In this work, a new unsupervised classification approach is proposed for the biomedical image segmentation. The proposed method will be known as Fuzzy Electromagnetism Optimization (FEMO). As the name suggests, the proposed approach is based on the electromagnetism-like optimization (EMO) method. The EMO method is extended, modified, and combined with the modified type 2 fuzzy C-Means algorithm to improve its efficiency especially for biomedical image segmentation. The proposed FEMO method uses fuzzy membership and the electromagnetism-like optimization method to locate the optimal positions for the cluster centers. The proposed FEMO approach does not have any dependency on the initial selection of the cluster centers. Moreover, this method is suitable for the biomedical images of different modalities. This method is compared with some standard metaheuristics and evolutionary methods (e.g. Genetic Algorithm (GA), Particle Swarm Optimization (PSO), Electromagnetism-like optimization (EMO), Ant Colony Optimization (ACO), etc.) based image segmentation approaches. Four different indices Davies–Bouldin, Xie–Beni, Dunn and β index are used for the comparison and evaluation purpose. For the GA, PSO, ACO, EMO and the proposed FEMO approach, the optimal average value of the Davies–Bouldin index is 1.833578359 (8 clusters), 1.669359475 (3 clusters), 1.623119284 (3 clusters), 1.647743907 (4 clusters) and 1.456889343 (3 clusters) respectively. It shows that the proposed approach can efficiently determine the optimal clusters. Moreover, the results of the other quantitative indices are quite promising for the proposed approach compared to the other approaches The detailed comparison is performed in both qualitative and quantitative manner and it is found that the proposed method outperforms some of the existing methods concerning some standard evaluation parameters.

© 2020 Elsevier B.V. All rights reserved.

1. Introduction

Digital image processing has widespread applications in various domains like agriculture, security, medical domain, industrial

* Corresponding author.
E-mail addresses: shouvikchakraborty51@gmail.com (S. Chakraborty), kalyanimali1992@gmail.com (K. Mali).

https://doi.org/10.1016/j.asoc.2020.106800
1568-4946/© 2020 Elsevier B.V. All rights reserved.

applications, etc. Image segmentation plays a vital role and required as the preliminary step in most of the applications of digital image processing [1]. Image segmentation is considered as one of the challenging tasks in the field of computer vision. The main job is to automatically divide an image into its constituting regions based on the gray level intensity or the values of the Red, Green, and Blue channels (in case of a color image). The integration of the segments should produce the actual image. The segmented regions must possess some similarities. Similarities can be measured based on different features like color, texture, intensity, or something else. This similarity can also be computed using some mathematical functions. Biomedical image segmentation is an important step in computer-aided diagnostic processes. In general, biomedical images suffers from several problems like poor quality and correlation, ambiguous overlapping regions, noise, etc. and these problems makes the job more difficult for the physicians. Biomedical image segmentation is a useful tool to detect various abnormalities like abnormal tissue growth, infections, foreign objects, etc. [2,3]and it is also helpful for the precise and quick investigations of different parts of the body. Anatomical structures can be easily studied with the help of automated image segmentation. Pathologists, microbiologists, etc. can take advantage of the biomedical image segmentation methods in cell counting, detecting the presence of viruses, microbes, classification of diseases, etc. [4,5]. Therefore, automated image segmentation methods have a significant impact in the field of biomedical image analysis and can make significant progress in this domain which is necessary for providing accurate and timely treatment to the patients [4,6]. Biomedical image segmentation is one of the major processes to get information about the different internal organs of the body in a non-invasive manner and therefore segmentation plays a vital role in different medical applications like analysis and exploration of anatomical structures, simulation of different biological mechanisms, pathological investigations, disease analysis, and progression tracking, assessing the condition and the requirement of surgery and many more. With the advancement of technology, computer-aided diagnostics systems are getting improved day-by-day and advanced image segmentation approaches become an inevitable part of these systems. Moreover, different operational functionalities are highly dependent on the performance of the associated image segmentation procedure. From this discussion, it can be understood that the task of segmentation demands some sophisticated methods to identify various sections of an image. As discussed earlier, there are some inherent problems which are associated with the biomedical images, and in many occasions, it has been observed that the crisp segmentation approaches cannot efficiently and precisely determine the segmented regions from the biomedical images and hence, the prime goal of this research work is to develop a fuzzy method that can effectively and reliably determine the segments from the biomedical images of different modalities with the help of the EMO algorithm.

Image segmentation is one of the prime research areas which is being addressed by many researchers of various domains. A single solution is not enough to apply to all types of images. Some prominent issues of digital images like poor contrast, uneven intensity distribution, poor illumination, ambiguous boundaries, etc. make the problem difficult and hard to analyze [7–10]. Therefore, the crisp method may not be suitable always to segment such types of images [8]. The theory of the fuzzy sets can help in this issue [11]. Here, the basic concept is one point can belong to more than one cluster with some degree of membership [12]. The sum of all the membership values for a particular point must be 1 and this type of membership is known as the partial membership [13]. The degree of membership is decided by the fuzzy membership functions and based on this theory

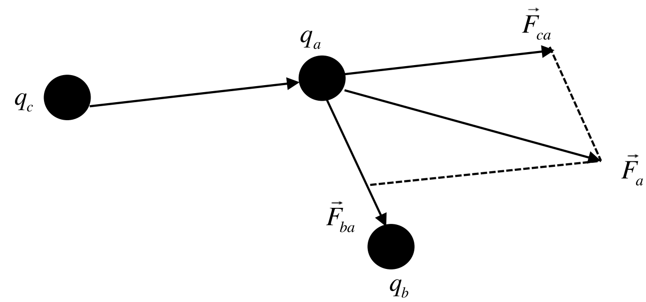

Fig. 1. Explanation of the superposition principle in EMO method.

many difficult problems are solved. Image segmentation is no exception and exploits the concept of the fuzzy set theory to find various regions of an image. Using the concept of fuzzy set theory, the popular fuzzy C-means [14] clustering method is developed and it has a widespread applications not only in image segmentation but, many other fields are also using this concept [6,15]. The major advantages of the fuzzy C-means clustering method are, this method can retain more information than the crisp clustering method and suitable for the overlapped datasets because a data point can belong to more than one cluster with some degree of membership. This method is robust and gives better performance than the K-means method for those images where the prominent overlapped regions can be observed. The generalized version of type 1 fuzzy set which is nothing but the type 2 fuzzy set, is adapted in this work. In normal fuzzy C-means clustering method, the cluster centers are dependent on the mean of all its constituting points. It can be easily understood that the final clustering outcome is heavily dependent on the selection of the initial cluster centers which is a major problem associated with this. This work designed a biomedical image segmentation method called Fuzzy Electromagnetism-like Optimization (FEMO) that uses the type 2 fuzzy set theory [16] and electromagnetism-like optimization [10]. Electromagnetism-like optimization can be used to solve global optimization problems. This method is based on electromagnetism and the behavior of the charged particles. This method mimics the attraction and the repulsion mechanism of the charged particles.

The electromagnetism-like optimization method is used to solve different problems of various domains. In [17], authors proposed a solution to segment white blood cells from microscopic images using electromagnetism-like optimization methods. The circle detection problem is used to find white blood cells using the electromagnetism-like optimization method. The objective function is designed in such a way so that it can find the similarity between a probable circle and the shape of the white blood cells. The proposed method is tested with some problems of different levels of complexity and the experimental results prove its efficiency and the real-life applicability. A neural-fuzzy system optimization based on the EMO method is proposed in [18]. The proposed method is used to solve the nonlinear system identification and classification problems. In this work, the population size is dynamic and it is decided based on the similarity measure. The EMO method is combined with the gradient descent method to improve the convergence. Its performance and efficiency can be judged from the experimental results. The EMO algorithm is applied on the project scheduling problem in [19]. In this work, a resource-constrained environment is selected. Different types of instances are used to test this method and a consistently good performance can be achieved. This work also gives a future research direction to apply this method in other domains. The EMO method is hybridized with the migration strategy and applied

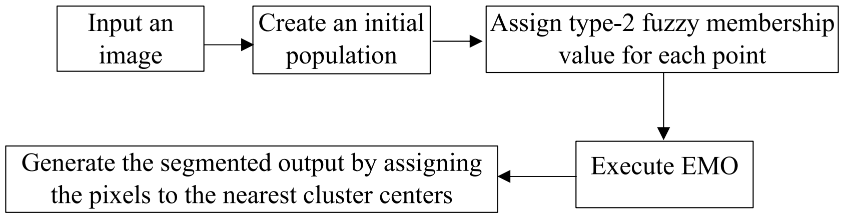

Fig. 2. Simple flow diagram of the proposed system.

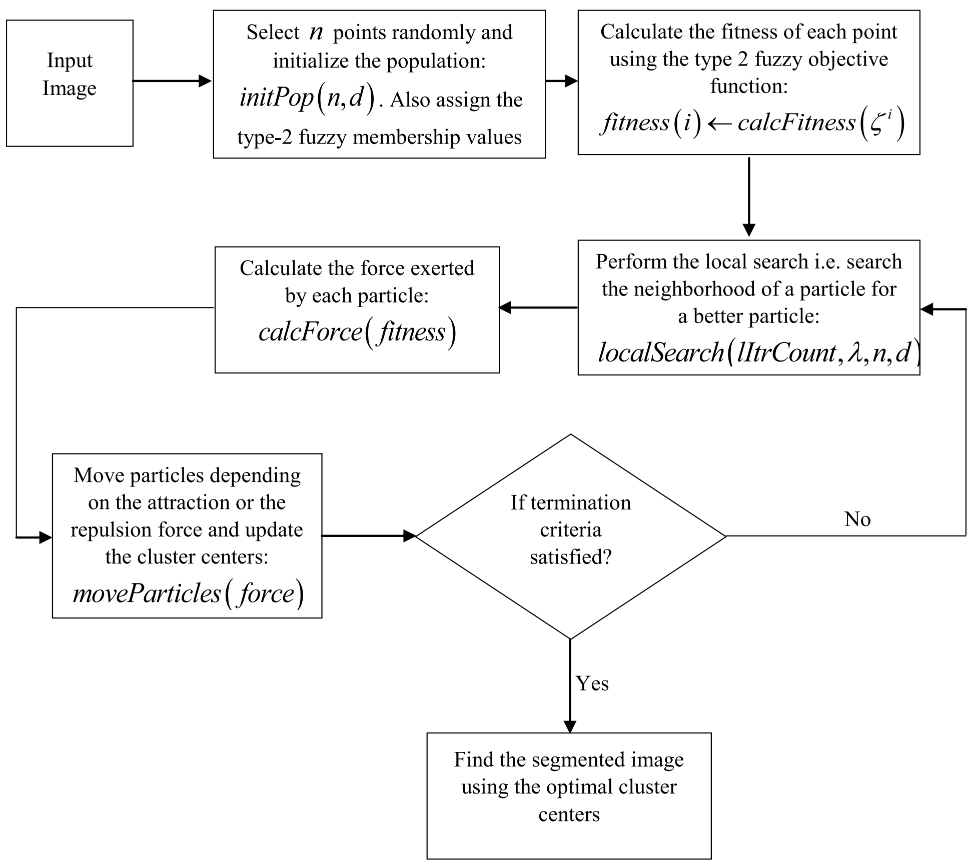

Fig. 3. The flow diagram of the proposed FEMO method.

to optimize the truss structures. This hybrid algorithm is used to update the positions of the particles and to reach the global optimum. The truss structure optimization problem is solved by the proposed method considering some frequency constraints. The experimental results show the practical applicability of this proposed algorithm. In [20], a constraint handling technique is proposed for the EMO algorithm. This method can be used to solve various practical engineering design problems. Each iteration of this method is supported using a derivative-free searching mechanism to improve the convergence. This method is tested and compared with some stochastic methods using some engineering problems. A modification of the local search method in the EMO algorithm is proposed in [21]. The proposed local search is implemented using the chaotic optimization procedure and this modified EMO is tested using some problems and the results are compared with the actual EMO process to prove its efficiency. The EMO algorithm is applied in [22] to produce isospectral non-uniform beams corresponding to a given uniform beam. The authors propose an error function to compute the separation between the spectra of the uniform and the non-uniform beam and this difference is minimized using the EMO method. Experimental results prove the presence of the isospectral non-uniform beams corresponding to a uniform beam as a local optimum. Moreover, structural damages are also detected in this work by finding the isospectral non-uniform beams corresponding to a damaged beam using the EMO method. A modification to the EMO algorithm is proposed in [23] to optimize the fractional-order PID. The proposed method is named the IEMGA i.e. 'improved EM algorithm with genetic algorithm technique'. Here the different controller parameters are used as the charged particles. The local search procedure is implemented using the genetic algorithm and this improvement reduces the computational complexity of the overall system. The performance of the proposed method is illustrated using many examples. A binary version of the EMO method is proposed in [24] to determine the solution of the combinatorial optimization problems. This method is applied to solve the traveling salesman problem and the results are compared with some of the standard methods of the literature to prove the superiority. The EMO algorithm is used to optimize electromagnetic devices in [25]. The proposed method is demonstrated by optimizing the pole faces of a magnetizer. These optimal pole faces are required to generate the necessary magnetic flux density distribution. A novel application of the EMO algorithm can be found in [26] where the EMO is used for the feature selection purposes. Here

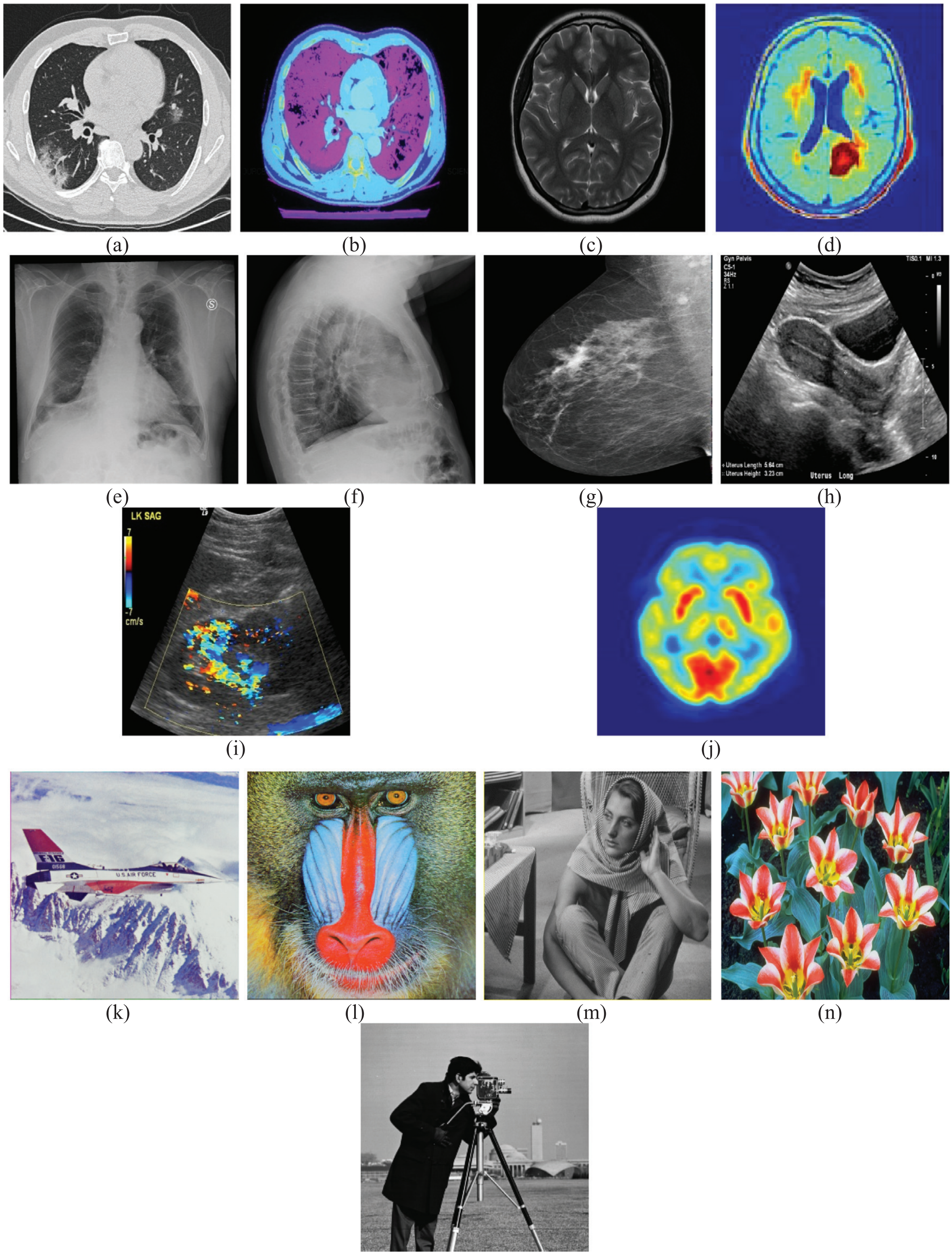

Fig. 4. Original biomedical images and standard test images under consideration (a) CT Scan image (grayscale)-I_{001}, (b) CT Scan image (color)-I_{002}, (c) MRI image (grayscale)-I_{003}, (d) MRI image (color)-I_{004}, (e) X-ray Image (grayscale) PA view-I_{005}, (f) X-ray Image (grayscale) Lateral view-I_{006}, (g) Mammogram (grayscale)-I_{007}, (h) Ultrasonic image (grayscale)-I_{008}, (i) Ultrasonic image (color)-I_{009}, (j) PET image (color)-I_{010}, (k)–(o) Standard test images Airplane-I_{011}, Baboon-I_{012}, Barbara-I_{013}, Tulips-I_{014} and cameraman-I_{015} respectively.

one nearest neighbor (i.e 1NN) is used with the EMO method for feature selection and classification. The main criterion for feature selection is the minimum rate of miss-classification. Various types of datasets are used to prove the efficiency of the proposed method. This method proves to be effective compared to some other standard methods in terms of both classification and feature selection and the practical application of this method is demonstrated using a real-life dataset of gestational diabetes mellitus. A modification of the multi-objective optimization method (MOEM) based on the EMO method is proposed in [27]. In this work, the proposed MOEM method is compared with some of the standard multi-objective optimization methods and the Pareto fronts

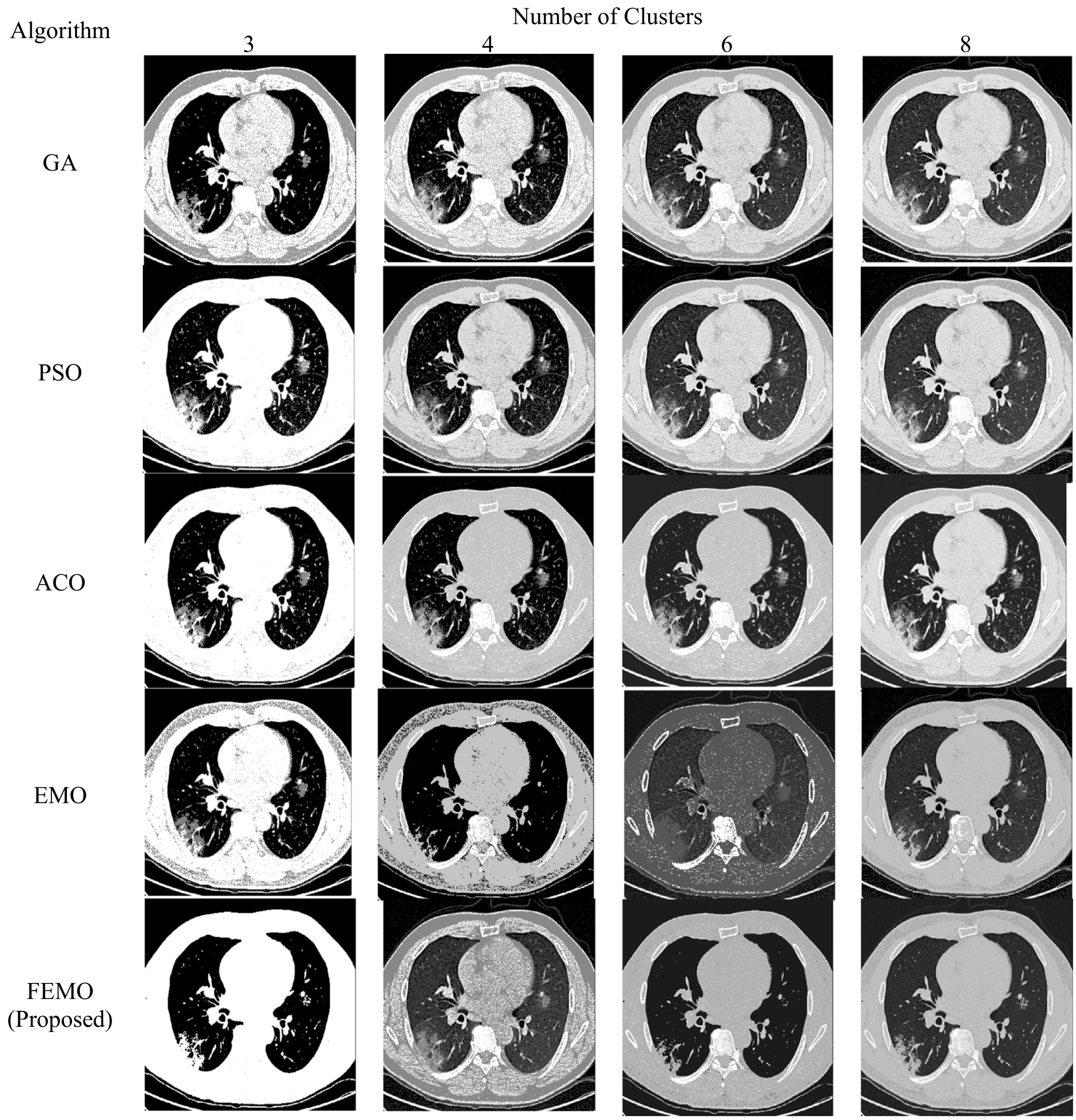

Fig. 5. Segmented output of the CT Scan image (grayscale) (Fig. 4(a)-I_{001}) obtained using different methods and for different no. of clusters.

are compared and proved that the proposed method is a good competitor of existing multi-objective optimization algorithms. Apart from these approaches, a hybrid ant swarm optimization approach which is known as the immune ant swarm optimization is proposed in [28]. The ant swarm optimization is a hybridization of the ant colony optimization and particle swarm optimization. This approach preserves the convergence of the global search in PSO. This approach is the combination of the PSO, ACO and the immune approach which helps obtain better optimal rough reducts, 12 benchmark datasets are incorporated in this work for the experiments and evaluation purposes and the proposed approach generates some encouraging results. A grey wolf optimizer (GWO) based solution is designed for the path planning problem and for a Proportional–Integral (PI)-fuzzy controller tuning problem in [29]. The experiments are performed to evaluate the proposed approaches in a single multiagent environment with nRobotic platform. The experimental approaches prove the effectiveness and improvement in the performance of the GWO based solution for the path planning problem and tuning the Proportional–Integral (PI)-fuzzy controller.

The proposed FEMO method incorporates the concept of type 2 fuzzy sets with EMO method and it is applied in biomedical image segmentation. As discussed earlier, the proposed algorithm helps to determine the segments without having any sensitivity to the selection of the initial cluster centers. The number of the parameter for the EMO method is quite reasonable compared to many other metaheuristic algorithms. The EMO method can reach the global optima even after getting stuck in a local optima [30,31]. The attractive region of the population is thoroughly examined by the EMO method which is a major advantage of this method [30]. So, the advantages of both type 2 fuzzy set and the EMO method are exploited in this method to get better segmentation results and this is the basic motivation behind this work. Some biomedical images with different modalities are successfully segmented by the proposed method. The efficiency of the proposed FEMO method is analyzed by both visual and numerical methods. Some well-known cluster validity indices are used for this purpose.

Various real-life problems involve multiple-variable based non-linear functions. Moreover, these functions may contain some attributes like multimodality, discontinuity, etc. Stochastic search approaches are proved to be efficient in solving these problems [32]. It is worth mentioning in this context that the discrete optimization problems are harder to solve compared to the

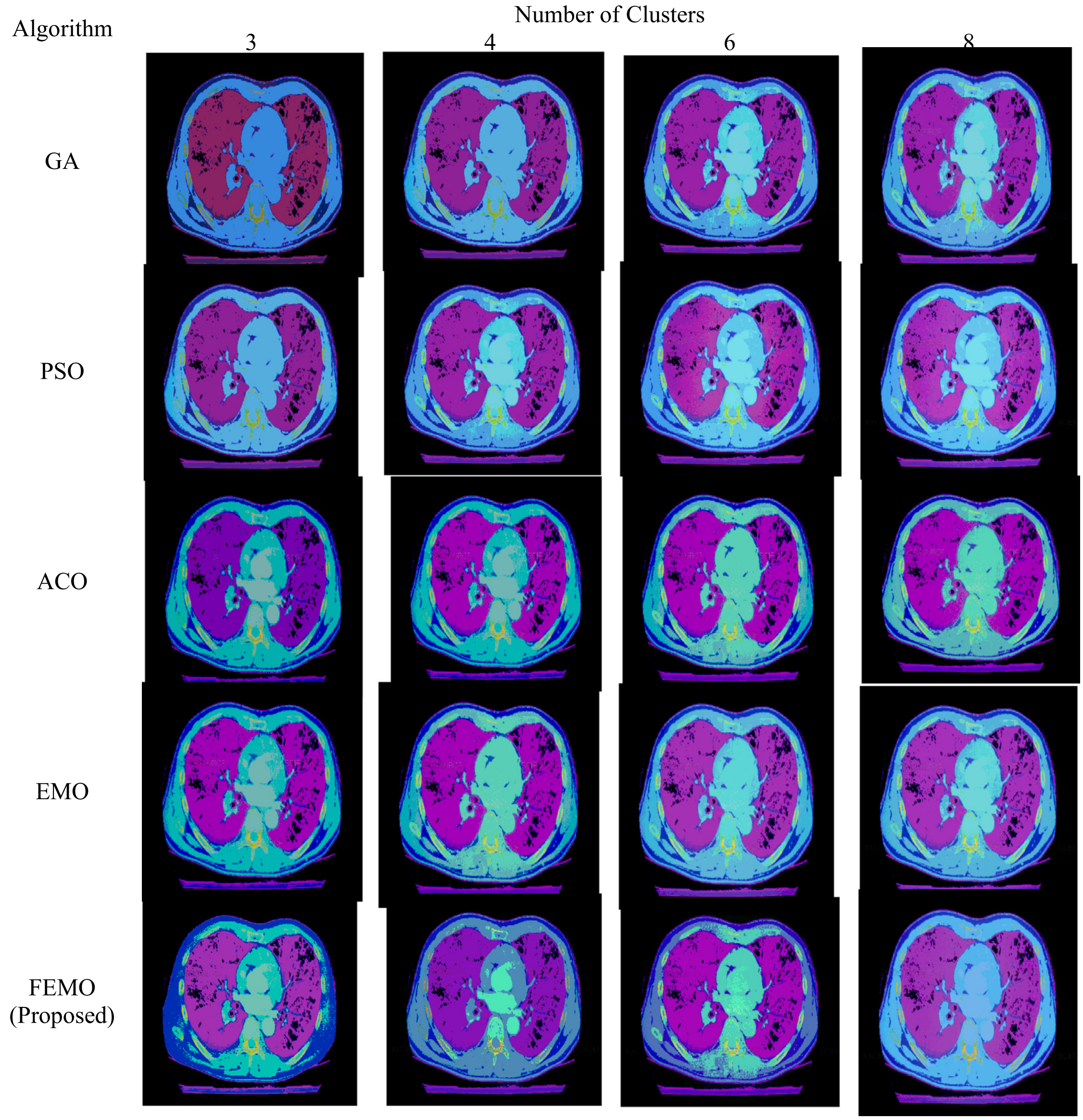

Fig. 6. Segmented output of the CT Scan image (color) (Fig. 4(b)-I_{002}) obtained using different methods and for different no. of clusters.

continuous optimization problems [33,34]. Typically, population-based optimization approaches begin by taking a short sample from the possible solution space. The value of the fitness function is determined for each solution and the domain of preference is determined based on the fitness function. The probable candidate domains are further exploited by certain mechanisms like reproduction, mutation, and crossover in the case of genetic algorithms. The electromagnetism-like optimization approach is inspired by the attraction–repulsion mechanisms of the electromagnetically charged particle. In this approach, each data point is considered as the charged particle. Apart from performing the global search, the EMO approach incorporates a local search procedure to exploit the neighborhood of the best solution discovered. It allows an efficient way to search for the total solution space. The performance of the EMO method is evaluated and compared in [35]. It can be observed that the performance of the EMO method is quite better compared to some other standard approaches. It inspires us to design a new approach based on the EMO method and applied on the biomedical images and the obtained results are quite promising. The incorporation of type 2 fuzzy system helps to efficiently model various real-life scenarios and the associated uncertainties. Therefore, the proposed FEMO approach is helpful to realistically model the problem of biomedical image segmentation because biomedical images often suffer from poor correlation, overlapping regions without proper boundary line, poor contrast etc. There are several metaheuristic approaches that can be found in the literature which is dedicated to certain types of applications [13,36,37]. In general, there are no concrete and universal algorithm or method that can determine the suitable algorithms for a specific approach. The decision can only be made on the basis of the quantitative and qualitative experiments [38–43].

The proposed FEMO approach is used for the biomedical image segmentation purposes and four existing approaches like genetic algorithm (GA) [44], particle swarm optimization (PSO) [45], electromagnetism-like optimization (EMO) [17], ant colony optimization (ACO) [46] are used to evaluate and demonstrate the comparative performance using the both qualitative and quantitative manner. In this work, the segmented outcomes are not compared with any manual delineations. However, the proposed work can perform the job of segmentation without having any knowledge about the ground truth data. To demonstrate the effective performance of the proposed approach further and to make the results more reliable, some standard test images are

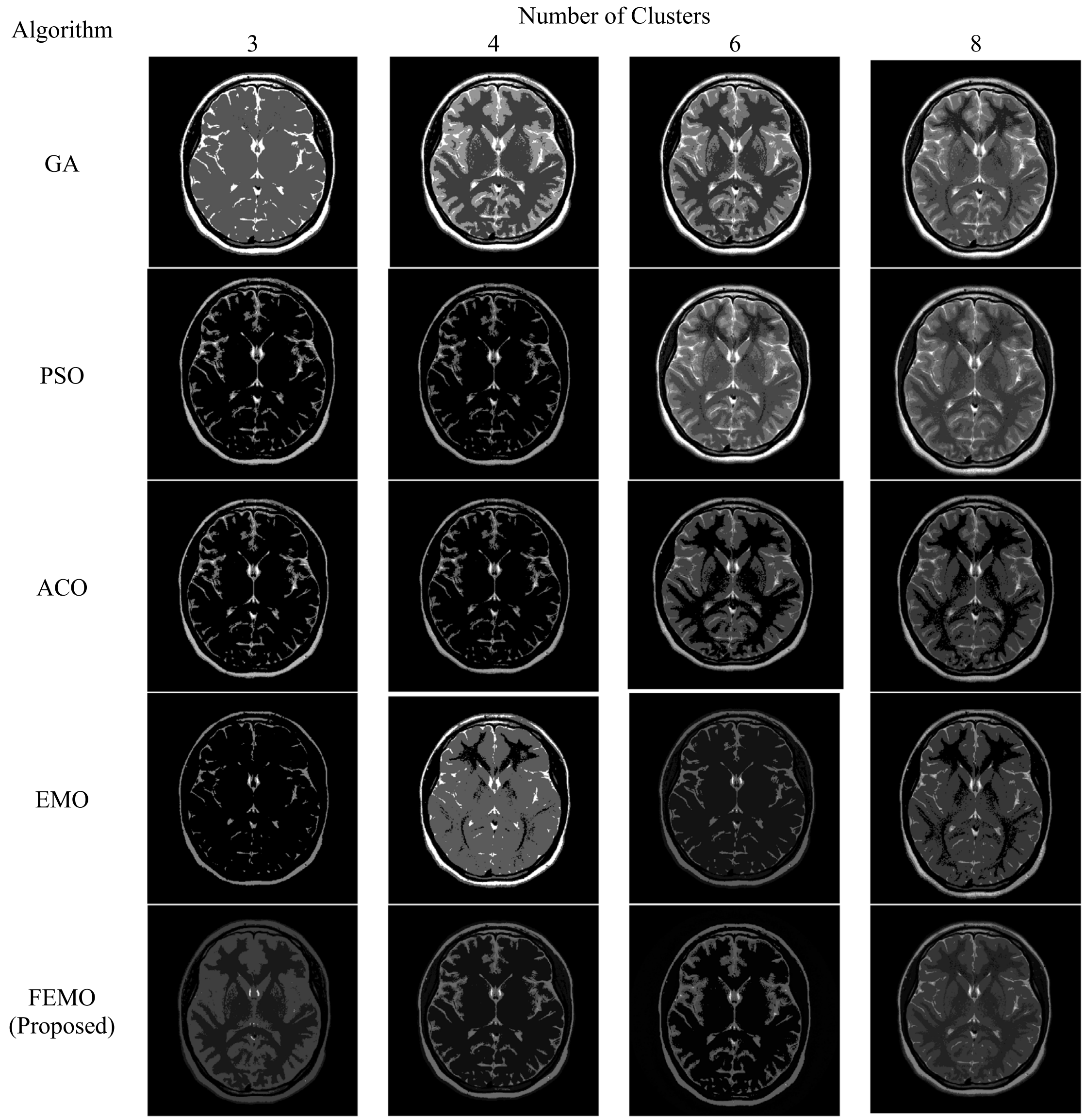

Fig. 7. Segmented output of the MRI image (grayscale) (Fig. 4(c)-I_{003}) obtained using different methods and for different no. of clusters.

also incorporated in the revised article. The proposed approach and the other four approaches are applied to these standard test images and the value of the four validation indices are reported for the different number of clusters. The segmented outputs are also reported which are useful for the visual investigations. The obtained results are found to be quite promising and establish the efficiency of the proposed FEMO approach in both a qualitative and quantitative manner. The overall average values of the four quantitative validation metrics are reported at the bottom of every table to get a glimpse of the overall performance of the proposed system compared to other approaches.

The remaining article is organized as follows. Sections 2 and 3 briefly illustrates the concept of electromagnetism-like optimization method and the type 2 fuzzy set respectively and gives a hint of how these two methods can be unitedly applied for the image segmentation purpose. Section 4 describes the proposed method. Section 5 shows the obtained results and their interpretation. Section 6 presents some of the limitations of the proposed approach. Section 7 concludes this article and Section 8 discusses some important and interesting points and also gives some future directions on it.

2. The electromagnetism-like optimization (EMO) method

Electromagnetism-like optimization method is first proposed in [30] and it can be used for the global optimization purposes. This method mimics the attraction–repulsion mechanism of the charged particles as per the theory of electromagnetism. The basic electromagnetism-like optimization method is described in Algorithm 1. This method works in four distinct phases. In the first phase of the algorithm, some points are randomly selected from the search space to initialize the population. In the second phase, this method looks for the local optimum. This step requires a local search procedure that can be achieved using different methods like simulated annealing [47], hill-climbing [48], gradient descent method [49] etc. the third stage uses superposition theory of the electromagnetism [50] to calculate the exerted force by each points. The amount of charge and the distance between two points are the necessary parameters which are used to compute the force. This concept is demonstrated in Fig. 1. Here, $\vec{F}_{ca}$ is the force which is experienced by q_a and exerted by q_c. Here, q_a is repulsed by the q_c. In EMO method, it is possible when, the fitness value of q_a is better than the q_c. $\vec{F}_{ba}$ is the force

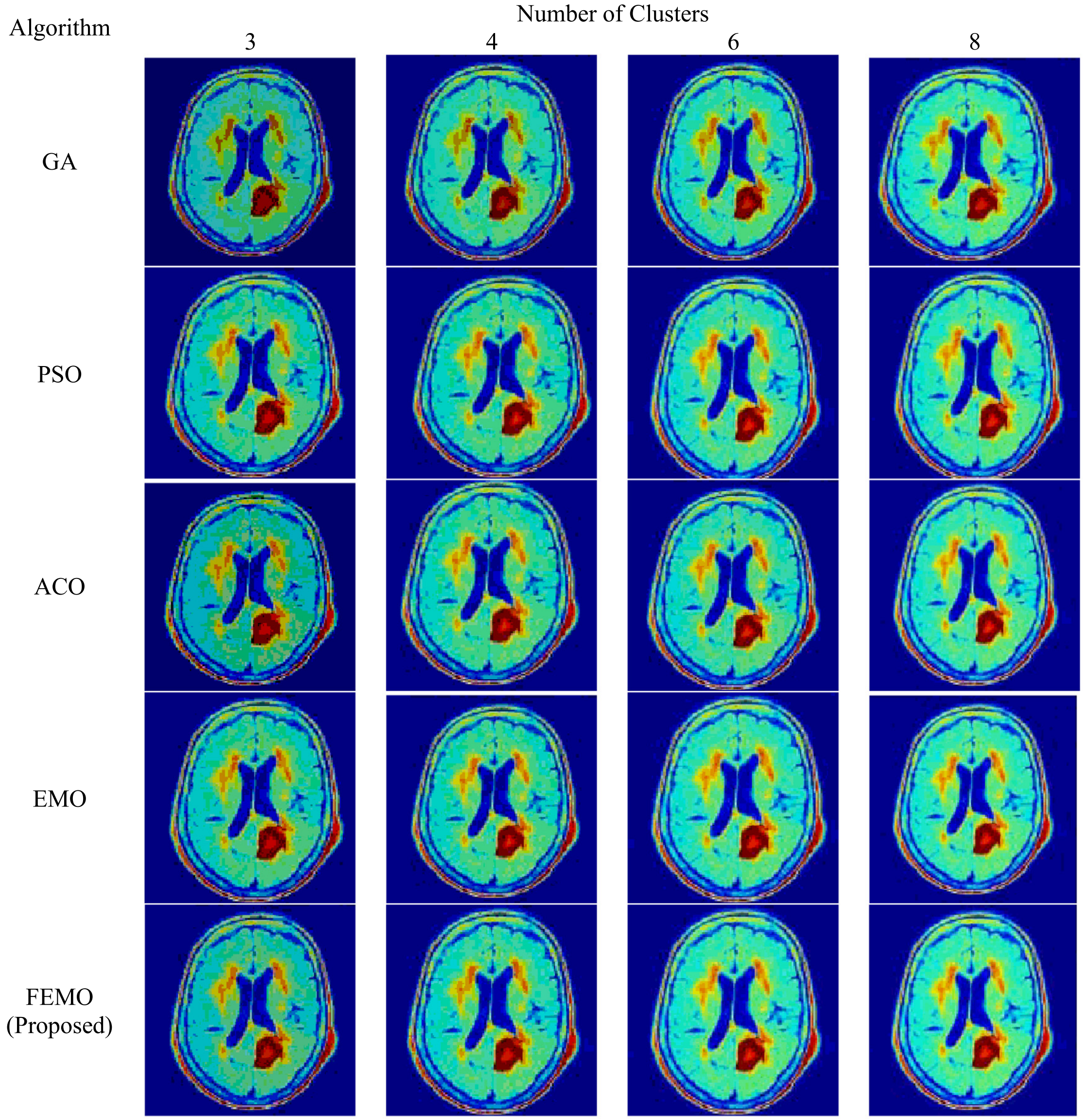

Fig. 8. Segmented output of the MRI image (color) (Fig. 4(d)-I_{004}) obtained using different methods and for different no. of clusters.

which is experienced by q_a and exerted by q_b. In this case, q_a is attracted by the q_b. From perspective of the EMO method, this phenomenon indicates that the fitness value of q_b is better than q_a. The resultant force, which is experienced by q_a can be represented as $\vec{F}_a = \vec{F}_{ca} + \vec{F}_{ba}$. So, in the EMO process, each point is treated as the charged particles with attraction or repulsion forces with respect to other particles. Here, the amount of charge represents the fitness value for that particle. A particle with better fitness value can attract other particles and a particle with worse fitness value can repel other particles. So, in the third phase, the cumulative force experienced by a particle due to the attraction and repulsion of other particles is computed in this phase. In the fourth phase, the particle is moved towards the direction of the force. From the second to the fourth stage is repeated while the termination criteria are satisfied. This process can be terminated if the maximum number of iterations is reached. This process can also be terminated if the state of the points does not change in two or more than two successive iterations.

The EMO algorithm can solve nonlinear optimization problems (which have a form like Eq. (1) with a box constraint) and can reach the global optimum.

$$\max f(t), \quad t = (t_1, t_2, t_3, \ldots\ldots, t_n) \in \mathbb{R}^n \textit{ subject to } t \in T \tag{1}$$

Here, $f : \mathbb{R}^n \rightarrow \mathbb{R}$ denotes a non-linear function and $T = \{t \in \mathbb{R}^n | lb_k \le t_k \le ub_k,\ k = 1, 2, 3, \ldots\ldots, n\}$ is a bounded region and the bounds are the two constraints, upper bound and lower bound, and these are represented by lb_k and ub_k respectively.

3. The type-2 fuzzy set and clustering

The fuzzy C-means (FCM) clustering method is one of the most popular and frequently used clustering approaches in the literature [51]. Unlike crisp clustering methods, it allows a data point to be part of more than one cluster with some membership values. The membership value for a point decides the level or a degree of a point that belongs to a certain cluster. This value is known as the degree of membership. The summation of all the membership values for a point must be 1. FCM method has a widespread application and frequently adapted to solve various problems in the field of computer vision and pattern recognition. Fuzzy clustering approaches are useful and can efficiently solve various problems which are may not be solvable by the crisp clustering approaches [52]. The objective function which is optimized by the fuzzy c-means clustering method is given in Eq. (2). The centers of the clusters are computed by minimizing this function.

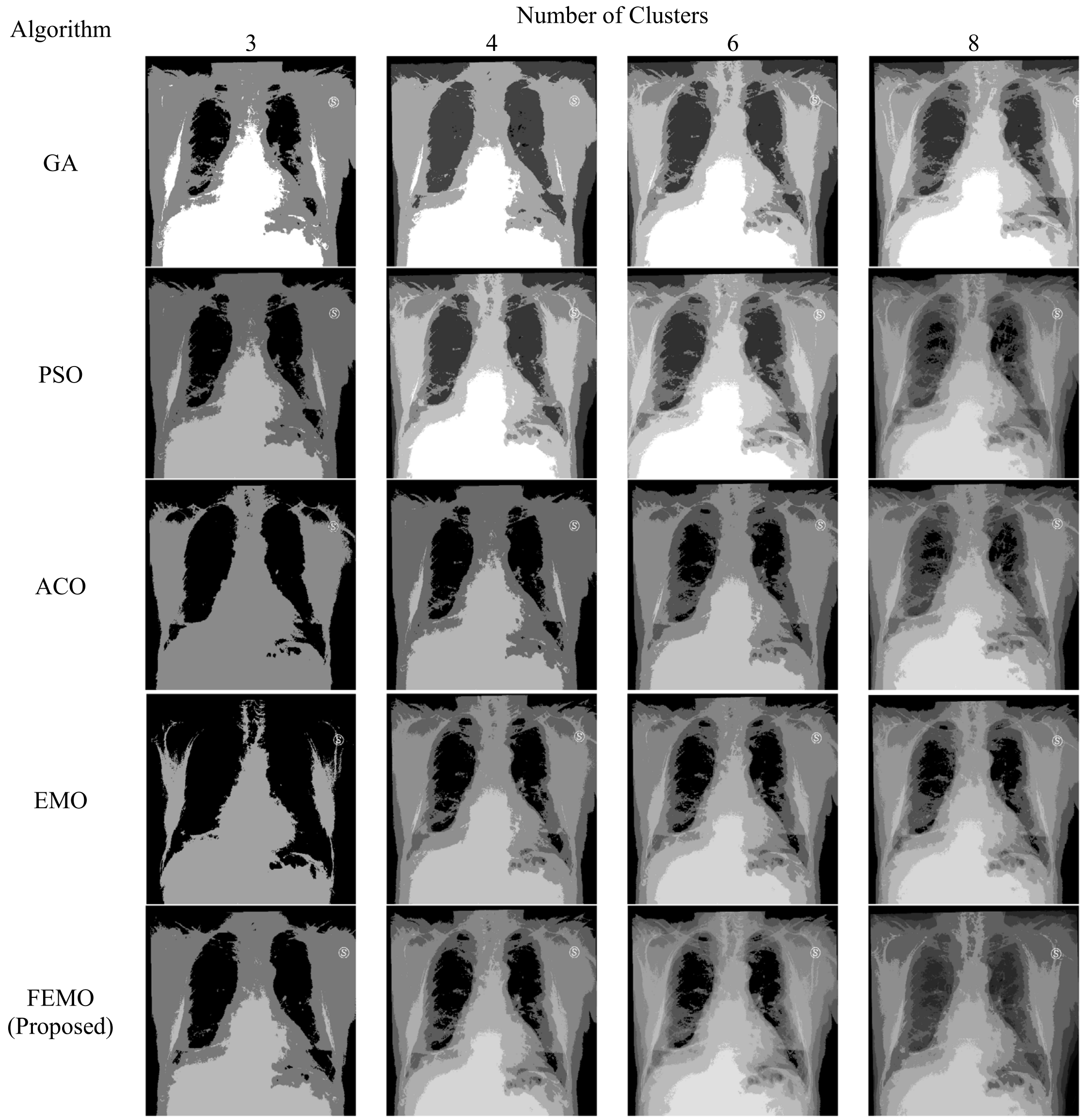

Fig. 9. Segmented output of the MRI X-ray image (grayscale) PA View (Fig. 4(e)-I_{005}) obtained using different methods and for different no. of clusters.

Algorithm 1: The electromagnetism-like optimization (EMO) method

---

Inputs: The size of the initial population SZ. The maximum number of iterations $gItrCount$. The maximum number of iterations for the local search $lItrCount$. The local search parameter $\lambda \in [0,1]$.

Output: Optimal result(s)

1: $initPop(\;)$: Initialize the population

2: $fitness \leftarrow calcFitness(\;)$: compute the fitness value for each particle

3: $localSearch(lItrCount, \lambda)$: perform the local search

4: $force \leftarrow calcForce(fitness)$

5: $moveParticles(force)$: move the particles depending on the exerted force

6: Repeat step 3 to 4 until the termination criteria is satisfied.

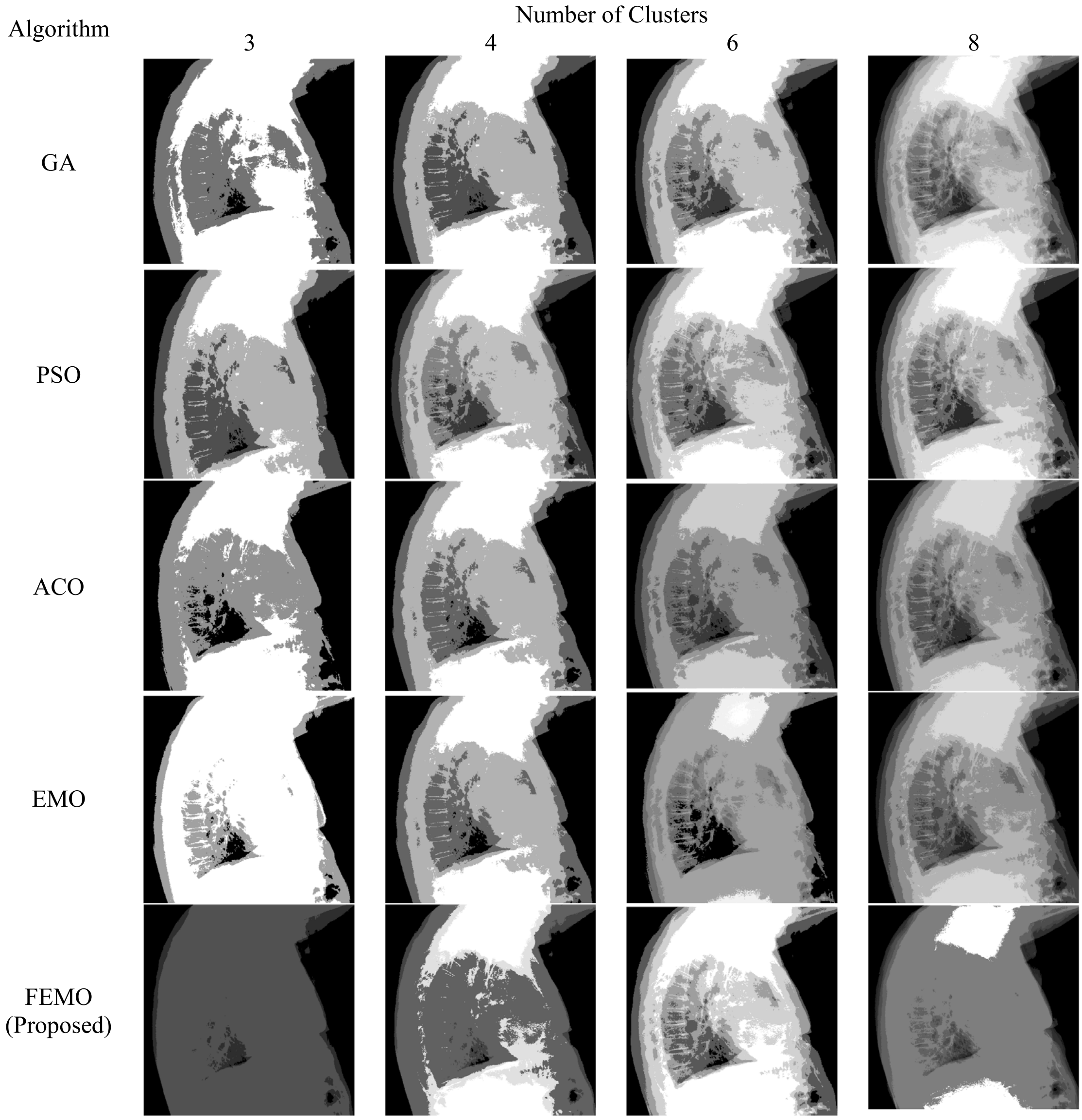

Fig. 10. Segmented output of the MRI X-ray image (grayscale) Lateral View (Fig. 4(f)-I_{006}) obtained using different methods and for different no. of clusters.

This dissimilarity function is used by the traditional type 1 FCM clustering method as the objective function. The cluster centers are updated using Eq. (4).

$$J_q = \sum_{i=1}^{P}\sum_{j=1}^{M}\mu_{ij}^{q}\left\|x_i - c_j\right\|^2, \ \ where\ 1 \le q < \infty \tag{2}$$

Eq. (3) expresses the μ_{ij} and it denotes the degree of membership of point x_i to the jth cluster. As discussed earlier, for a certain point, the summation of μ_{ij} must be 1 i.e. $\sum_{i=1}^{c}\mu_{ij} = 1\ for\ j = 1, 2, 3, \ldots\ldots., n$. x_i is the k dimensional data point c_j represents the k dimensional cluster center. P is the number of data points and M is the number of clusters.

$$\mu_{ij} = \frac{1}{\sum_{l=1}^{c}\left(\frac{\|x_i - c_j\|}{\|x_i - c_l\|}\right)^{\frac{2}{q-1}}} \tag{3}$$

$$c_j = \frac{\sum_{i=1}^{P}\mu_{ij}^{q}x_i}{\sum_{i=1}^{P}\mu_{ij}^{q}} \tag{4}$$

This error function used to compute the degree of membership. It is a squared function and used by the traditional type 1 fuzzy clustering system. The fuzzy type 1 clustering system suffers from some inherent problems. The first problem is the noise. Fuzzy type 1 clustering system is heavily affected by noise and therefore not suitable for the applications in biomedical image analysis [53]. Sometimes, relative membership values creates some difficulties and restricts it from being applied in various problems [54]. Motivated from this, the type 2 fuzzy system is adapted and combined with the EMO algorithm [55]. From the above discussions, one thing is very clear that if the membership value for a certain point for a cluster is very high i.e. close to 1 then, the uncertainty of that point is reduced because the membership value 1 indicates the complete involvement of a point to a particular cluster. Similarly, the uncertainty of a point increases with the lesser value of the membership i.e. closer to 0. So, the points with lesser uncertainty (i.e. with higher membership value) have more chance of participation and, the points with higher uncertainty (i.e. with lesser membership value) have a lesser chance of participation. This concept is exploited by the type 2 fuzzy systems and the advantages are given below [55]:

a. The points with the lesser degree of the membership (i.e. with higher uncertainty) have a comparatively lesser

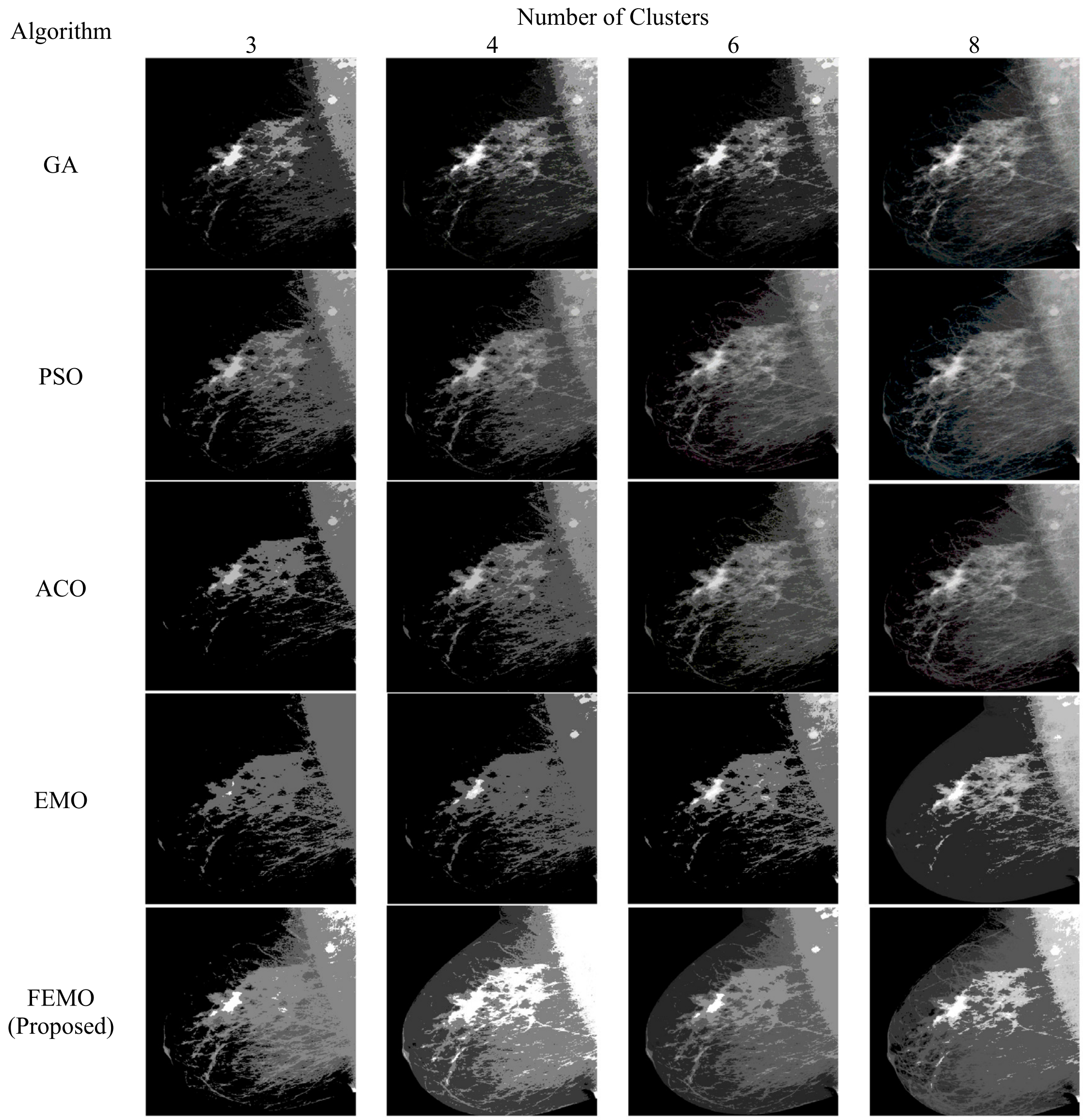

Fig. 11. Segmented output of the mammogram image (grayscale) MLO view (Fig. 4(g)-I_{007}) obtained using different methods and for different no. of clusters.

effect on a cluster center than a point with a higher degree of membership (i.e. with lesser uncertainty). Therefore, if the degree of membership for a certain point tends to 0 then the effect of that point on the cluster center almost vanishes. This concept is very useful and well suited to solve various real-life problems.

b. As discussed earlier, noise handling is a major challenge in type 1 fuzzy systems. Type 2 fuzzy systems can handle the noise more effectively that the type 1 fuzzy systems. More realistic and stable cluster centers can be achieved with the help of type 2 fuzzy clustering systems. Incorporating the type 2 fuzzy system in the fuzzy C-means clustering method requires the concrete definition of the membership function. The membership values can be considered as the weights and can be computed using Eq. (5) where the value of μ_{ij} is the degree of membership which is obtained using Eq. (3).

$$\gamma_{ij} = \mu_{ij} - \frac{1-\mu_{ij}}{2} \tag{5}$$

From Eq. (4), it is evident that the type 2 fuzzy clustering system is a function of type 1 fuzzy clustering system. Now, the fuzzy type 2 membership γ_{ij} can be replaced in Eq. (4) and the modified equation to update the cluster centers can be written as Eq. (6).

$$\tilde{c}_j = \frac{\sum_{i=1}^{P} \gamma_{ij}^{q} x_i}{\sum_{i=1}^{P} \gamma_{ij}^{q}} \tag{6}$$

Type 2 fuzzy clustering system is simple to implement and well suited to model various practical problems. This method is adopted in this work because it can produce better segmentation results due to its efficient noise handling capability [55]. The type 2 fuzzy C-means based clustering method is illustrated in algorithm 2. This procedure starts by initializing the degree of membership for the input data points. Initially, the degree of membership for each point is initialized randomly and the total sum of the membership values for a certain point must be 1. A threshold value is supplied to the algorithm which is useful to check whether the procedure can be stopped or not. Actually, if the difference in the fitness value of the objective function in the ith iteration and the $(i+1)$th iteration is greater than or equal to the threshold value then, the process repeated otherwise the process can be terminated. Therefore, this threshold value can be used as a termination criterion and the quality control

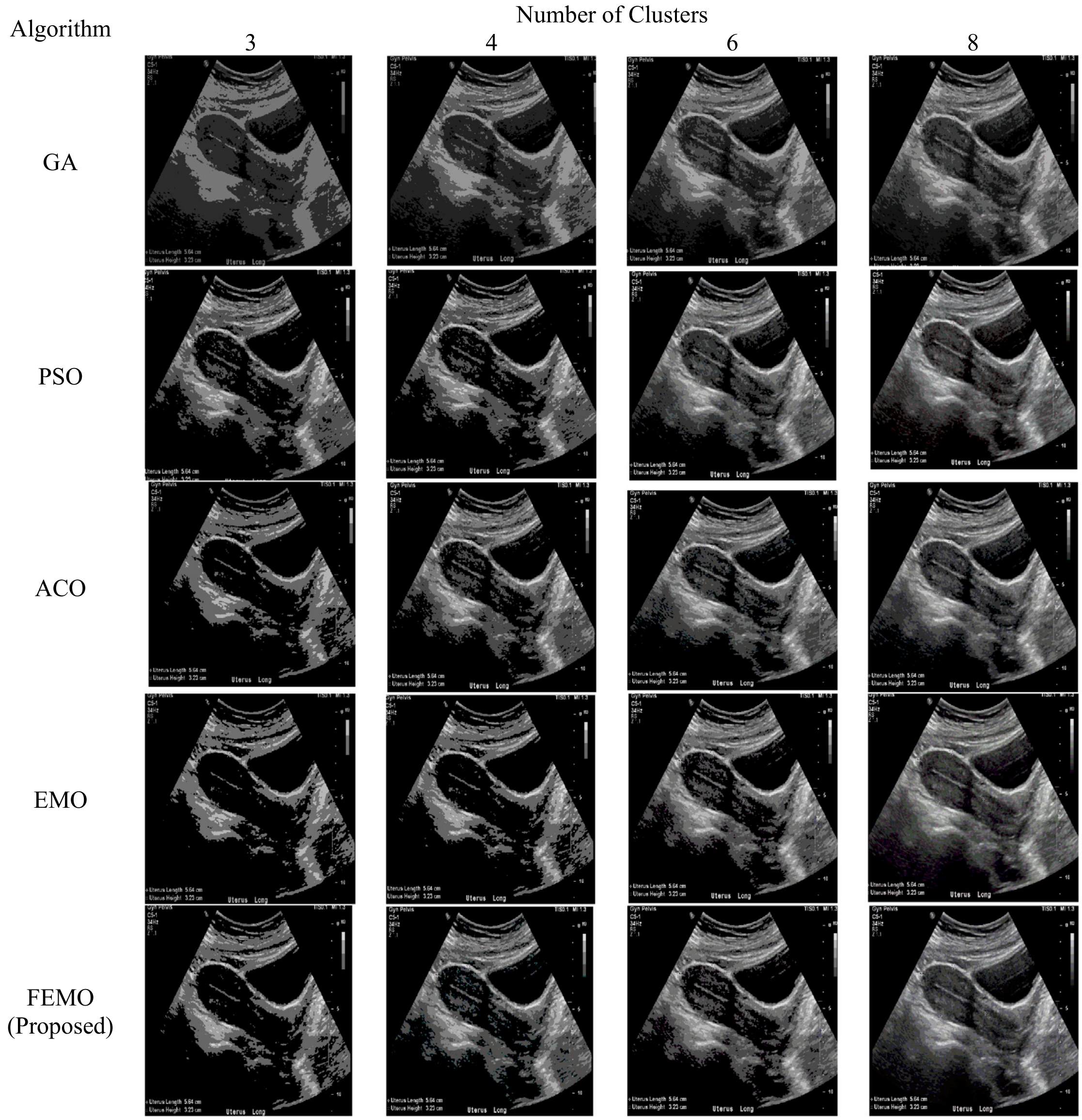

Fig. 12. Segmented output of the USG (grayscale) (Fig. 4(h)-I_{008}) obtained using different methods and for different no. of clusters.

parameter for this clustering method. This algorithm improves the uncertainty handling capability of type 1 fuzzy clustering system apart from the increased efficiency from the perspective of noise handling.

4. The proposed FEMO method

The proposed method obtains the optimal clustering outcome by combining type 2 fuzzy C-means clustering with the electromagnetism-like optimization (FEMO) method and the name for this proposed method is given accordingly. The overall flow of the proposed system is depicted in Fig. 2. According to algorithm 1, the FEMO method starts by initializing the cluster centers in a random manner. The cluster centers are denoted as CC_i and $I_{low} \leq CC_i \leq I_{high}$, $i = 1, 2, 3, \ldots\ldots, n$. Here, I_{low} and I_{high} are the lowest and the highest intensities of the image under consideration and n is the number of cluster centers. Eq. (7) can be helpful to initialize the cluster centers. Here, *random* (0, 1) produce a uniformly distributed random number between 0 and 1.

$$CC_i = I_{low} + random\,(0,1)\left(I_{high} - I_{low}\right) \tag{7}$$

Table 1
Important parameters and their values in the proposed FEMO method.

Name of the parameter	Value
Number of populations n	20
gltrCount	300
lltrCount	40
The local search parameter λ	0.005

The objective function which is to be optimized by the FEMO method is given in Eq. (8).

$$J_i = \arg\min_{CC} \sum_{s=1}^{n} \sum_{t \in CC_j} \gamma_{st}^2 * D_{st} \tag{8}$$

Here, γ_{st} is the value of the membership that denotes the degree of membership of the tth pixel to the sth cluster in fuzzy type 2 system and it can be computed using Eq. (5) and D_{st} denotes the distance between them.

The proposed FEMO approach randomly initializes the cluster centers and guide them so that the it can reach the global optima. The optimization procedure guides the whole system to achieve

Algorithm 2: Type 2 fuzzy C-means based clustering

Input: The data points to be clustered and a threshold value th.

Output: Clustered data points

1: $\Upsilon \leftarrow initMembership(\ )$ random initialization of the membership values or the degree of memberships for the data points and for a certain point, the sum of all the membership values must be 1.

2: The cluster centers can be located using equation 6.

3: Compute the fitness value using the objective function which is given in equation 2.

4: Check if $improvement \geq th$ then

a. Determine the value of γ_{ij} using 5

b. Goto step 2 and repeat again

end if

5: Return the clustered data points

Table 2
The description of the ten biomedical images and five standard test images which are selected for the testing purpose.

Image Id	Image	Source	Description
I_{001}	Computed Tomography (CT) Scan image (grayscale)	[56]	The CT Scan image (axial view) of the chest region. This image is collected from a 43 years old COVID-19 positive male patient from Italy. (Credit to R. Bonacini, G. Besutti, P. Pattacini Radiology IRCCS Reggio Emilia; Director Pierpaolo Pattacini).
I_{002}	Computed Tomography (CT) Scan image (color)	[57]	False color CT Scan image of the heart and the lungs region (axial view). Both heart and lungs are in normal state.
I_{003}	Magnetic Resonance Imaging (MRI) (grayscale)	[58]	A T2 weighted MRI image (axial view) of the head region of a 20 years old female patient. The patient was suffering from Vague headaches. (Case courtesy Associate Professor Dr. Frank Gaillard)
I_{004}	Magnetic Resonance Imaging (MRI) (color)	[59]	MRI color image of the head region (axial view)
I_{005}	X-ray Image (grayscale)	[60]	X-ray image of the chest region (PA view). This image is collected from a 70 years old COVID-19 positive male patient from Riccione, Italy. The patient was suffering from fever, cough, breathing difficulties. (Case courtesy of Dr Domenico Nicoletti, Radiopaedia.org, rID: 74724).
I_{006}	X-ray Image (grayscale)	[60]	X-ray image of the chest region (Lateral view). It is collected from the same source as described in I_{005}.
I_{007}	Mammogram (grayscale)	[61]	The mammogram of the right breast in MLO view. This image is collected from a 50 years old female patient.(Case courtesy of Dr Garth Kruger, Radiopaedia.org, rID: 21555)
I_{008}	Ultrasonic image (grayscale)	[62]	The case is collected from a 30 years old female patient of the pelvic region(Case courtesy of Assoc Prof Craig Hacking, Radiopaedia.org, rID: 43471)
I_{009}	Ultrasonic image (color)	[63]	Ultrasonic image of the lower of the left kidney.
I_{010}	Positron Emission Tomography (PET) image (color)	[64]	Positron Emission Tomography of the head region.
I_{011}	Airplane	[65]	Standard test image
I_{012}	Baboon	[65]	Standard test image
I_{013}	Barbara	[65]	Standard test image
I_{014}	Tulips	[65]	Standard test image
I_{015}	Cameraman	[65]	Standard test image

the optimal value of the objective function which is given in Eq. (8). Now, to update the cluster centers, Eq. (6) is not required here. The cluster centers will be updated by the FEMO process. Here, the EMO method is used to guide the cluster centers to reach the globally optimum state by optimizing Eq. (8). The FEMO process produces the optimal set of clusters that represents the segmented regions of the image. The clusters are formed by assigning the nearest points corresponding to a cluster center. Type 2 fuzzy set is helpful in better convergence of this method in presence of noise [66].

After the initialization is over then, the fitness value for each member of the population is computed using Eq. (8) and the member with the best fitness values is stored in the ζ^{best}. The initialization process is elaborated and can be easily understood from algorithm 3.

In the next phase, the local information about a particle ζ^{i} is gathered using a maximum of *lItrCount* number of iterations. The local search parameter $\lambda \in [0, 1]$ and the *lItrCount* is used to perform this local search procedure. The local search method begins by finding the maximum possible step length using the local

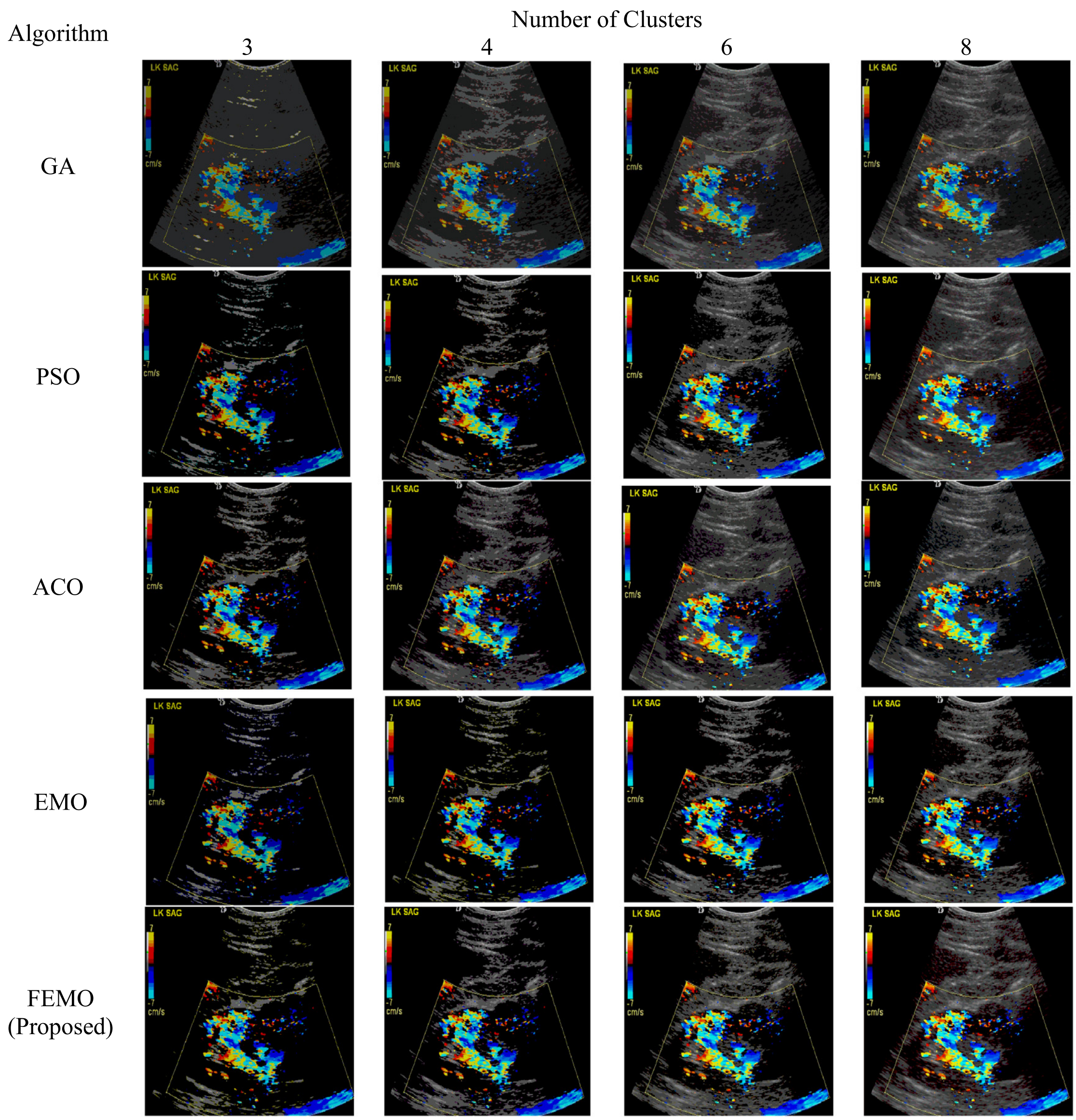

Fig. 13. Segmented output of the USG (color) (Fig. 4(i)-I_{009}) obtained using different methods and for different no. of clusters.

search parameter λ. The information about a cluster center i.e. a particle ζ^i is temporarily stored in a point κ. κ is moved along the direction of a selected random number. If better point can be achieved within the *lItrCount* number of iterations then, the point ζ^i will be replaced by κ and the search can be terminated. The ζ^{best} is updated with the current best fitness value which is obtained at the end of this process. The local search method is illustrated in algorithm 4. After the local search procedure, the resultant force is computed for each particle. The force exerted by a particle is determined with the help of the superposition principle [67]. According to this theorem, the exerted force by a particle due to another particle is directly proportional to the product of the number of charges and inversely proportional to the amount of distance between them. Here, the charge of a particle is mimicked by the fitness value of the corresponding solution i.e. the fitness value of a point is used to compute the charge of a particle. The value of the charge for a particle determines the attraction and the repulsion power of that particle. The charge ch^i for the ith particle can be computed using Eq. (9).

$$ch^i = e^{\left(-d\cdot\frac{calcFitness(\xi^i)-calcFitness(\xi^{best})}{\sum_{c=1}^{n}\left(calcFitness(\xi^c)-calcFitness(\xi^{best})\right)}\right)}, \quad \forall i \tag{9}$$

Therefore, a higher charge of a point indicates better fitness value and vice-versa. The dimension d is multiplied to make this equation computational friendly in higher dimension and to avoid overflow problems. One important point that can be observed from Eq. (9) is that, no sign is associated with it. The force exerted by a point p, $\vec{F}_p$, due to all other points can be expressed by Eq. (10). A point with better fitness value compared to the other points attracts others and a point with lesser fitness value compared to the other points repels others. The attraction and the repulsion mechanism between two points is implemented by comparing the fitness values of both the points. The point ζ^{best} is the point with the best fitness value (in this work, it is point with minimum fitness value) and therefore, it will attract all other points towards it. Here, the distance is computed using the Euclidean distance measure. The direction of the movement of a point is highly dependent on the points which are close to each other. Algorithm 5 will demonstrate this concept in detail.

$$\vec{F}_p = \sum_{q\neq p}^{n} \begin{cases} (\zeta^q - \zeta^p)\,\frac{ch^p ch^q}{\|\zeta^q-\zeta^p\|^2}\ if\ calcFitness(\zeta^q) \\ \quad < calcFitness(\zeta^p) \\ (\zeta^p - \zeta^q)\,\frac{ch^p ch^q}{\|\zeta^q-\zeta^p\|^2}\ if\ calcFitness(\zeta^q) \\ \quad \geq calcFitness(\zeta^p) \end{cases}, \quad \forall p \tag{10}$$

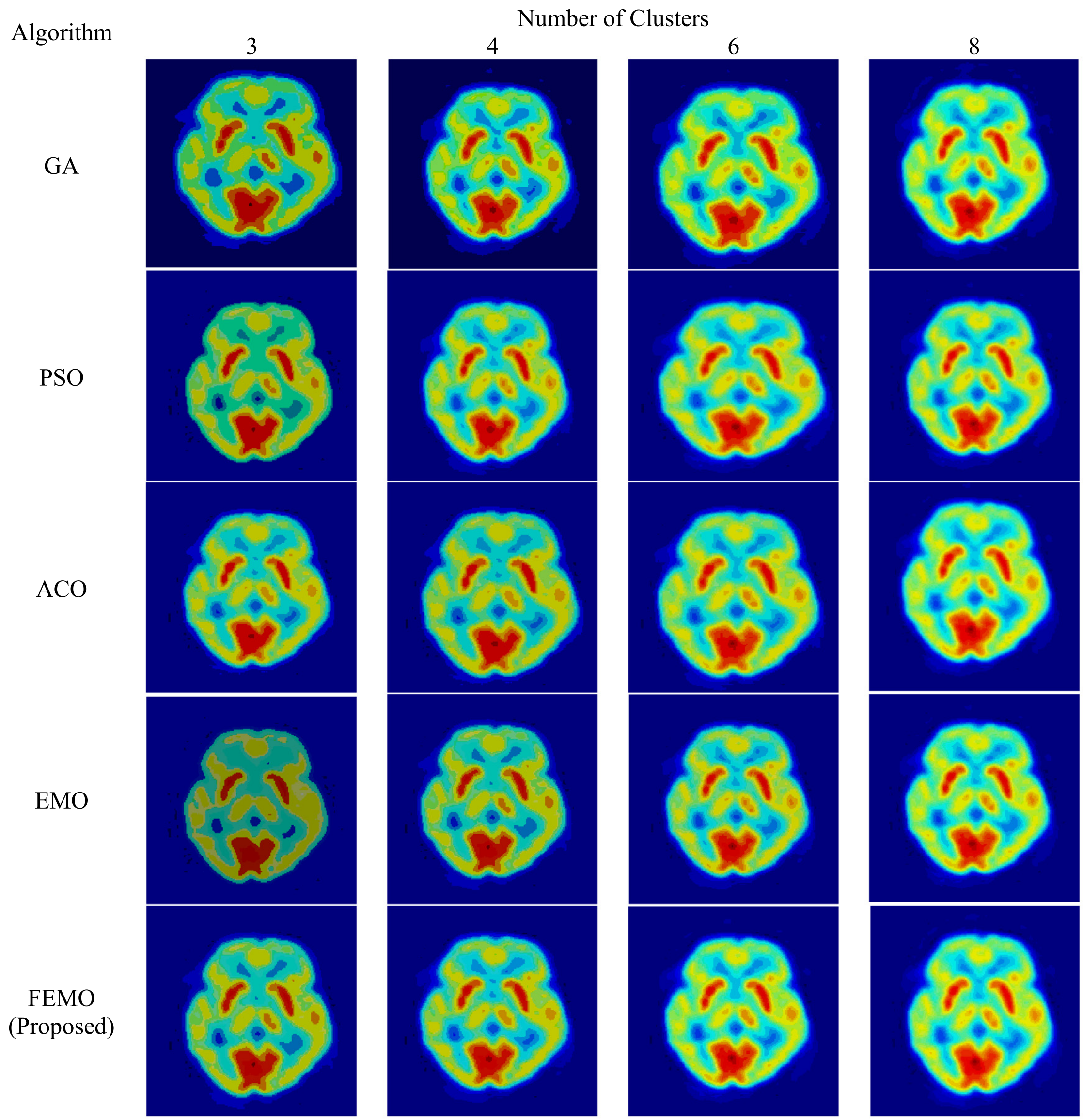

Fig. 14. Segmented output of the PET image (color) (Fig. 4(j)-I_{010}) obtained using different methods and for different no. of clusters.

In the next phase, the particles are moved according to their exerted force. A step length is computed in a random manner using Eq. (11). A uniformly distributed random value ε (between 0 and (1) is generated to compute the length of the steps. From Eq. (11), it can be clearly observed that the exerted force by a particle is normalized. $\vec{v}$ is a vector that contains the possible and allowed dimension wise movements towards I_{high} or I_{low}. The point with the best fitness value ζ^{best} is not moved and simply transferred to the next iteration and so on. Algorithm 6 illustrates this move procedure.

This movement procedure helps to adjust the cluster centers without explicitly using the equation to update the cluster centers. This procedure can be terminated if it reaches the optimal clustering outcome. However, it is not practical because the optimal clustering result is not possible to know beforehand. Therefore, the maximum number of iterations *gItrCount* can be used to terminate this process. Another possible termination criterion can be the optimum value remains constant in two or more successive iterations. It is an important point to be considered because to get the optimal results, the algorithm must not be stopped before the global optimum. Moreover, to reduce the overhead, unnecessary iterations are not at all desirable. The algorithm for the FEMO method is given in algorithm 7 and the flow diagram is given in Fig. 3.

One important point worth mentioning here is that no histogram-based operations are required here to perform the segmentation. The necessary parameters and their values that are used in this method is reported in Table 1. The efficiency and the real-life applicability of the proposed FEMO method is tested both visually and quantitatively. Some standard and well-known cluster validation measures are used for the experiment. The detailed results of the simulation are given in the next section.

The FEMO approach begins by initializing the cluster centers randomly using Eq. (7). This equation helps to initialize the cluster centers within the range of the gray-level intensity values. The initial solution space is guided further by the proposed FEMO approach to reach the global peak. After generating the points, the matrix Υ is prepared that contains the values of the degree of memberships using Eq. (5). It is obviously the type 2 fuzzy membership value. The values of the control parameters are used to control the overall functionality of the proposed system. The fitness is calculated using the objective function which is given in Eq. (8) and it is stored in a variable *fitness*. The definition of the

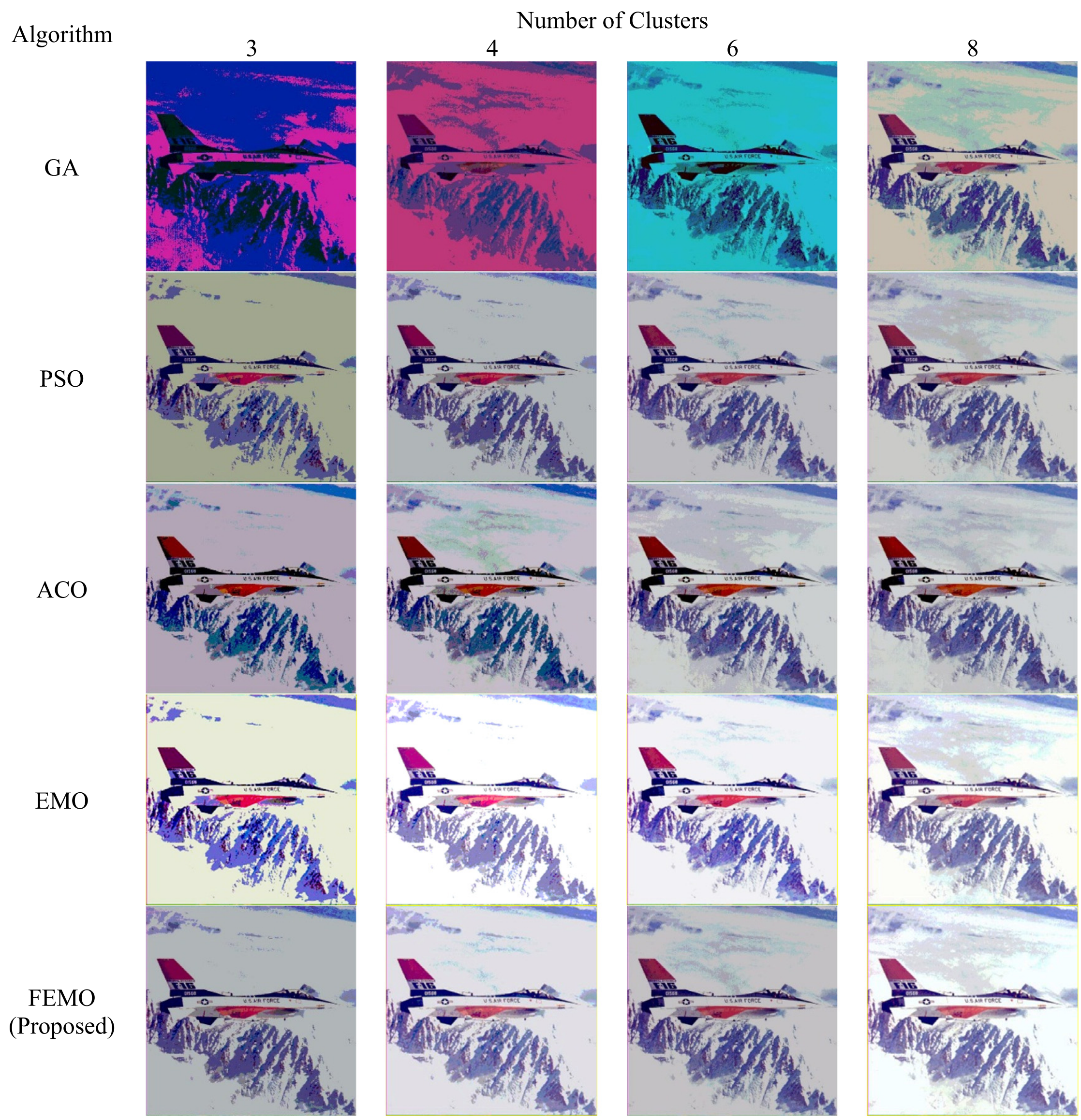

Fig. 15. Airplane image (color) (Fig. 4(k)-I_{011}) obtained using different methods and for different no. of clusters.

Algorithm 3: $initPop(n,d)$: Initialize the population

Input: Size of the population n and the dimension of each point d .

Output: Initial population and the best fitness value of this population ζ^{best}.

Repeat the following for $i = 1:n$ times
  Repeat the following for $j = 1:d$ times
    $\zeta_j^i = I_{low}^j + random(0,1)\left(I_{high}^j - I_{low}^j\right)$
  end for
  Compute the fitness of each point $fitness(i) \leftarrow calcFitness(\zeta^i)$
end for
$\zeta^{best} \leftarrow \arg\min\{fitness(i), \forall i\}$

Algorithm 4: $localSearch(lItrCount, \lambda, n, d)$: executes the local search method

---

Input: Maximum number of iterations $lItrCount$, the local search parameter $\lambda \in [0,1]$, Size of the population n and the dimension of each point d.

Output: Updated population and the best fitness value of this population ζ^{best}.

1: Set $cnt \leftarrow 1$
2: Set $len \leftarrow \lambda\left(\max_{j}\left\{I^{j}_{high} - I^{j}_{low}\right\}\right)$
3: Repeat the following for $i = 1 : n$ times
4: Repeat the following for $j = 1 : d$ times
5: Generate a random value $\tau_1 = random(0,1)$
6: Repeat the following steps while $cnt < lItrCount$
7: $\kappa \leftarrow \zeta^{i}$
8: Generate a random value $\tau_2 = random(0,1)$
9: Check if $\tau_1 > 0.5$ then
10: $\kappa_j \leftarrow \kappa_j + \tau_2(len)$
11: otherwise
12: $\kappa_j \leftarrow \kappa_j - \tau_2(len)$
end if
13: Check if $fitness(\zeta^{i}) > fitness(\kappa)$ then
14: $\zeta^{i} \leftarrow \kappa$
15: $cnt \leftarrow lItrCount - 1$
16: end if
17: $cnt \leftarrow cnt + 1$
end while
end for
end for
18: Compute the fitness of each point $fitness(i) \leftarrow calcFitness(\zeta^{i})$
19: $\zeta^{best} \leftarrow \arg\min\{fitness(i), \forall i\}$

---

objective function certainly varies depending on the underlying problem definition. One important point worth mentioning here is that the proposed approach can handle only one objective at a time. The *cntIteration* is a counter that takes care of the number of iterations and the total process is repeated for *gItrCount* number of times. A local search is performed *localSearch* (*lItrCount*, λ) to exploit the best solutions achieved so far. It is helpful in effectively reaching the global optimum. The maximum number of iterations for the local search is denoted by *lItrCount* and the local search parameter is denoted by $\lambda \in [0, 1]$. After performing the local search, the force exerted by each particle is computed using Eq. (10). Depending on the fitness values, two types of forces can be computed i.e. attraction or repulsion. Depending on these computed forces the particles are moved further. After getting the new positions of the particles, the cluster centers are updated and the value of type 2 fuzzy membership is also updated. The same process repeats until the maximum number of iterations are achieved.

The proposed FEMO approach is the modification of the actual EMO approach where the type 2 fuzzy system is incorporated. The proposed system has a strong theoretical background and can be applied in different scenarios. The proposed systems can efficiently handle the uncertainties with the help of the fuzzy type 2 system. This work is applied to the proposed FEMO approach for image segmentation purposes, to be more precise, for the biomedical image segmentation purpose. But from the discussion of the proposed approach, it can be understood that the proposed FEMO approach covers the total application domain of the actual EMO procedure. Moreover, it will be interesting to apply the proposed approach with or without modifications to some similar problems where the traditional crisp clustering approaches and their allied methods fail. Moreover, images with different application domains (e.g. satellite images) can also be segmented with some little modifications to the proposed approach.

5. Results of the simulation

In this section, the experimental results are discussed in detail. A comparative study is presented along with the detailed interpretation of the obtained results.

Algorithm 5: $calcForce(fitness)$: calculate force

Input: fitness of the points $fitness$.

Output: Computed force $\vec{F}$

Repeat for $i = 1 : n$ times
  Compute ch^i using equation 9
  $\vec{F}_i \leftarrow 0$
end for
Repeat for $i = 1 : n$ times
  Repeat for $i = 1 : n$ times
    If $fitness(j) < fitness(i)$ then
      $\vec{F}_i \leftarrow \vec{F}_i + (\zeta^j - \zeta^i)\dfrac{ch^i ch^j}{\|\zeta^j - \zeta^i\|^2}$ // Attraction force
    Otherwise
      $\vec{F}_i \leftarrow \vec{F}_i - (\zeta^j - \zeta^i)\dfrac{ch^i ch^j}{\|\zeta^j - \zeta^i\|^2}$ // Repulsion force
    end if
  end for
end for

Algorithm 6: $moveParticles(force)$: move particles depending on their exerted force

Input: Exerted force by each particle $force$

Output: Moved particles

Repeat for $i = 1 : n$ times
  Check if $i \neq best$ then
    $\varepsilon \leftarrow random(0,1)$
    $\vec{F}_i \leftarrow \dfrac{\vec{F}_i}{\|\vec{F}_i\|}$
    Repeat for $j = 1 : d$ times
      Check if $\vec{F}_i^j > 0$ then
        $\zeta_j^i \leftarrow \zeta_j^i + \varepsilon \cdot \vec{F}_i^j \cdot (I_{high}^j - \zeta_j^i)$
      Otherwise
        $\zeta_j^i \leftarrow \zeta_j^i + \varepsilon \cdot \vec{F}_i^j \cdot (\zeta_j^i - I_{low}^j)$
      end if
    end for
  end if
end for

Algorithm 7: Fuzzy Electromagnetism-like Optimization (FEMO) method-based image segmentation

Input: The size of the initial population SZ. The maximum number of iterations $gItrCount$. The maximum

Output: Optimal segmented output

1: $initPop(\ )$: Initialize the population
2: Set the values of the different input parameters (please refer table 1)
3: $\Upsilon \leftarrow initMembership(\ )$ random initialization of the membership values or the degree of memberships for the data points and for a certain point, the sum of all the membership values must be 1.
4: $fitness \leftarrow calcFitness(\ )$: compute the fitness value for each particle using the type 2 fuzzy objective function which is given in equation 8.
5: $cntIteration \leftarrow 1$
6: Repeat while $cntIteration \leq gItrCount$
7: $localSearch(lItrCount, \lambda)$: perform the local search
8: $force \leftarrow calcForce(fitness)$: calculate the exerted force by each particle using equation 10.
9: $moveParticles(force)$: move the particles depending on the exerted force and update the cluster centers.
10: Compute the fuzzy type 2 membership values
end while
11: Perform the segmentation based on the computed optimum cluster centers by assigning the points to their nearest cluster centers.
12: Display the segmented output

5.1. Description of the dataset

As discussed earlier, the proposed FEMO method is applied to the biomedical images for segmentation purposes. To test the effectiveness and the real-life applicability of the proposed method, biomedical images of different modalities are considered to perform the experiments. Both grayscale and the color images are segmented using the proposed biomedical image segmentation method. The images are consolidated from various sources. Table 2 gives an overview of the selected images along with their sources. 10 biomedical images are considered from different sources with modalities including both color and grayscale types to illustrates the versatility of the proposed FEMO method. Although the proposed approach is dedicated to the biomedical image data but, for the sake of completeness and to show the efficiency and the effectiveness of the proposed approach the experiments are carried out on some other standard image data. The segmentation output of these images is reported in Figs. 15 through 19. The corresponding quantitative results are reported in Tables 3 to 6. Fig. 4 shows the original images under consideration.

5.2. Cluster validity indices

Visual inspection of the segmented images is not sufficient the judge the quality of the segmented regions and in most of the scenarios, the actual interpretation of the segmented output remains incomplete without the quantitative analysis. Moreover, to compare the proposed work, only the segmented images are not sufficient and some numerical results are required. In this work, four well-known cluster validity indices are used to prove the efficiency of the proposed method as well as for the comparison purpose. The cluster validity indices are discussed below.

A. Davies–Bouldin index: It is the ratio of the sum of the intra-cluster distance and the inter-cluster distance [68]. To achieve a good clustering result, the inter-cluster distance must be high and the intra-cluster distance should be low and therefore, a lower value of the Davies–Bouldin index *DBInd* is desirable and indicates a good clustering result. Eq. (11) can be used to compute the value of this index. Here, denotes is the total count of the clusters. $p \neq l$ and the range of p is $1 \leq p \leq c$.

$$DBInd = \frac{1}{c}\sum_{p=1}^{c}\max\left(\frac{d_w\left(a_p\right)+d_w\left(a_l\right)}{d_b\left(a_p, a_l\right)}\right) \tag{11}$$

B. Xie–Beni index: It is one of the most popular indices to judge the quality of the fuzzy clustering [69]. The value of the Xie–Beni Index *XBInd* can be computed using Eq. (12). A smaller value of the *XBInd* indicates good clustering outcome.

$$XBInd = \frac{\sum_{q=1}^{c}\sum_{p=1}^{n}U_{qp}^2\left\|V_q - X_p\right\|^2}{d_{\min}\left\|V_q - V_p\right\|^2} \tag{12}$$

C. Dunn index: It is an important cluster validity index where the denominator contains the mean of the distances among all pairs of clusters and the numerator contains the distance between two clusters [70]. The value of the Dunn index can be computed using Eq. (13). Here, $d\left(c_i, c_j\right)$ is the distance between two clusters c_i and c_j. Δ_q denotes the mean of the distances among all pairs of clusters. The higher value of the Dunn index indicates better result.

$$DI_n = \min_{1\leq i\leq n}\left(\min_{1\leq j\leq n, j\neq i}\left(\frac{d\left(c_i, c_j\right)}{\max_{1\leq q\leq m}\Delta_q}\right)\right) \tag{13}$$

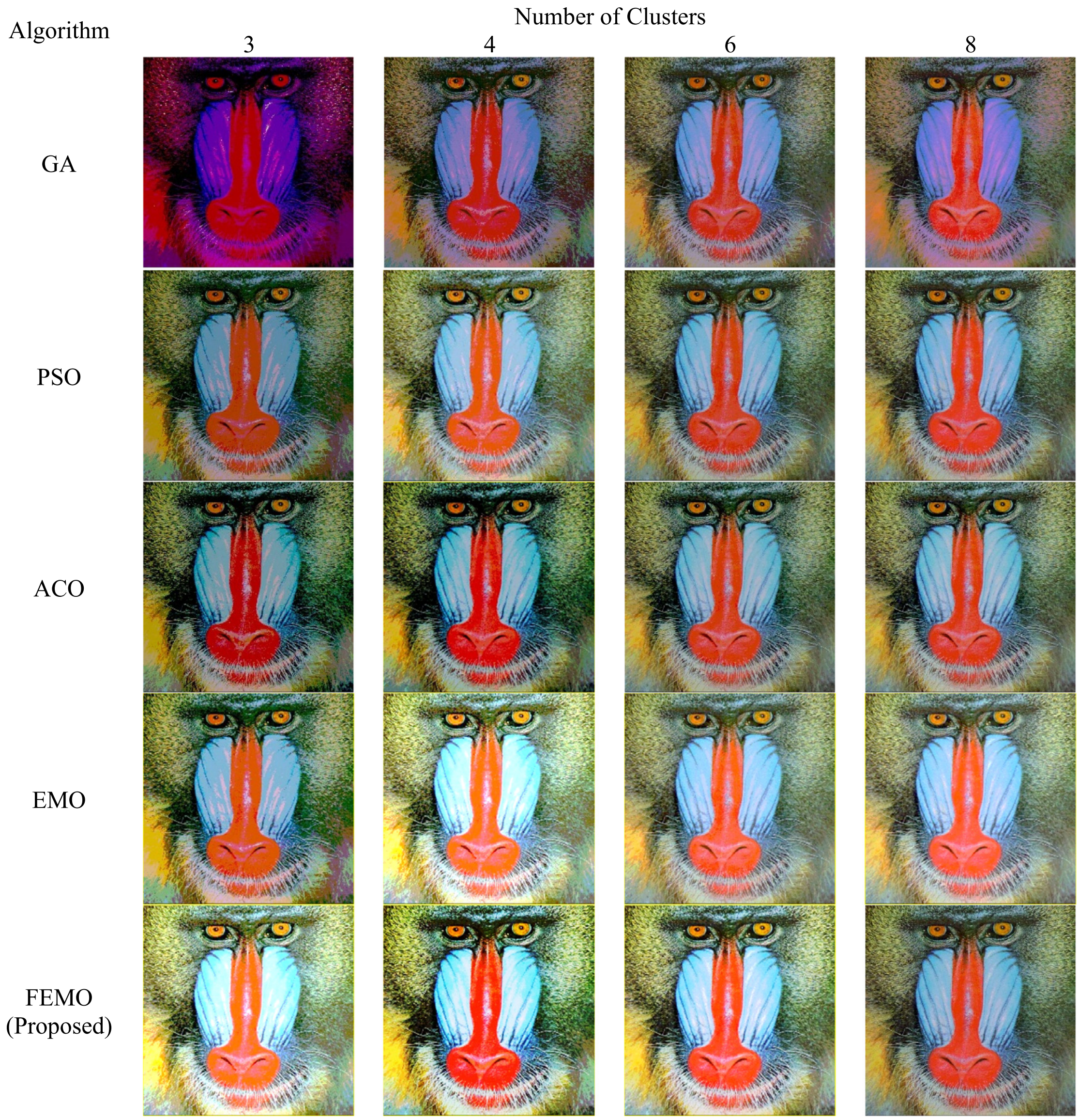

Fig. 16. Baboon image (color) (Fig. 4(l)-I_{012}) obtained using different methods and for different no. of clusters.

D. β **index:** The segmentation result can be evaluated by this index and it is defined in Eq. (14). The β index can be expressed as the ratio of the total variation to the inter-cluster variation [71]. Here, $cntP_s$ represents the count of the pixels in the sth cluster. I_{st} is the intensity of the tth pixel which belongs to the sth cluster. The mean of the intensity values in a cluster s is represented by $\hat{x}_s$. A well segmented set of clusters produces higher value of the β index.

$$\beta = \frac{\sum_{s=1}^{c} \sum_{t=1}^{cntP_s} (I_{st} - x)^2}{\sum_{s=1}^{c} \sum_{t=1}^{cntP_s} \left(I_{st} - \hat{x}_s\right)^2} \tag{14}$$

5.3. Results

The experiments are performed using MatLab R2014a (windows version) with an Intel i3 processor (1.8 GHz Clock Speed) and 4 GB of RAM in the Windows 7 environment. As discussed earlier, both qualitative and quantitative analysis is performed to test and compare the proposed algorithm with some other standard methods like genetic algorithm (GA) [44], particle swarm optimization (PSO) [45], electromagnetism-like optimization (EMO) [17], ant colony optimization (ACO) [46]. The proposed algorithm is tested and compared for the different numbers of clusters. Figs. 5–19 illustrates the comparative results of the segmentation by applying the proposed FEMO method and the other methods. The images are obtained by optimizing the Davies–Bouldin index by the various optimization methods.

5.4. Analysis of the convergence rate

Study of the convergence is one of the important parameters which is needed to be discussed to complete the analysis of an optimization procedure. In this work, the study of the convergence is performed using the first image i.e. with image id I_{001}. The Davies–Bouldin index is used to perform this study and the results are given in Fig. 20. The number of iterations vs. the value of the Davies–Bouldin index is plotted in each convergence curves which are given in Fig. 15. Different algorithms and for each of them, different numbers of clusters are compared. The graphical analysis is evident that the proposed FEMO method is effective and can be used to reach the global optimum in a reasonable amount of iterations. Moreover, the proposed FEMO

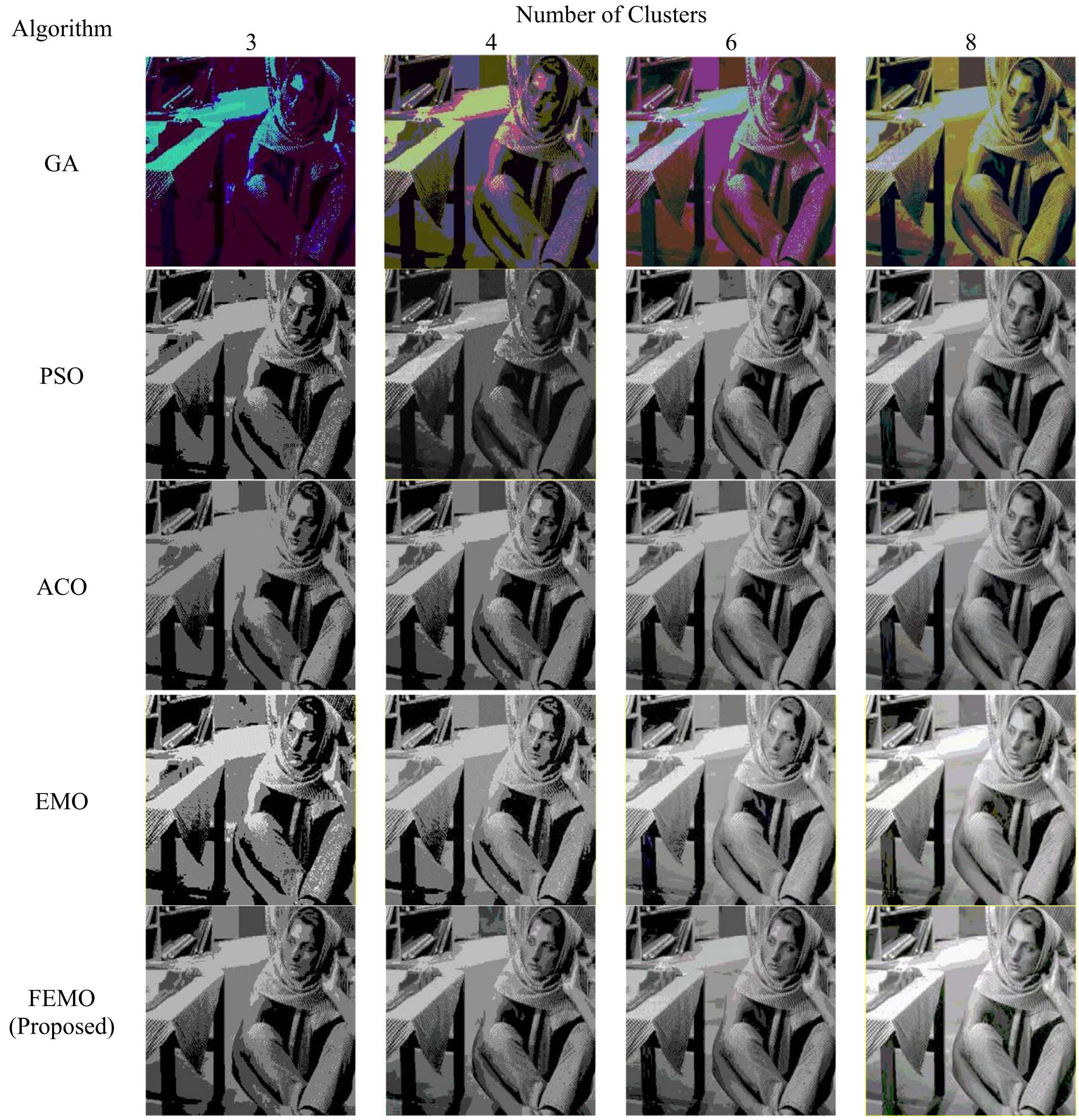

Fig. 17. Barbara image (grayscale) (Fig. 4(m)-I_{013}) obtained using different methods and for different no. of clusters.

method outperforms many standard methods in terms of the convergence.

The proposed approach is incorporating the type 2 fuzzy system with the EMO approach. The type 2 fuzzy system is helpful to model the uncertainties. The impact of the points which do not belong to a certain cluster creates a significant impact on finding the global optima. The proposed work addresses this problem. The proposed work can significantly diminish the impact of the points with very low membership values. The points with the lesser degree of the membership (i.e. with higher uncertainty) have a comparatively lesser effect on a cluster center than a point with a higher degree of membership (i.e. with lesser uncertainty). It helps to model various real-life problems efficiently and to reach global optima. The graphical analysis of the convergence is presented in Fig. 20 where the convergence curves for different approaches and the different number of clusters are presented that will provide a visual clue to analyze the convergence of the proposed work as well as some other works in the context of the biomedical image analysis.

6. Limitations of the proposed approached

The proposed approach is efficient enough to segment the biomedical images with different modalities but, the results will be more comprehensive if some more results are reported. The determination of the number of clusters is a challenging task and automated determination of the exact number of clusters can make the system robust but the proposed approach is not efficient enough to determine the number of clusters automatically which can be considered as the major drawback. The proposed approach is useful to optimize a single objective at any time. So the proposed approach cannot handle multiple objectives unless enhanced further. Besides some of these limitations, the proposed approach is efficient enough to segment the real-life biomedical images and the qualitative and quantitative results are helpful to show the efficiency of the proposed approach.

7. Conclusion

In this work, a new method of biomedical image segmentation is proposed where the advantages of the fuzzy type 2 clustering system and the EMO method is exploited to perform

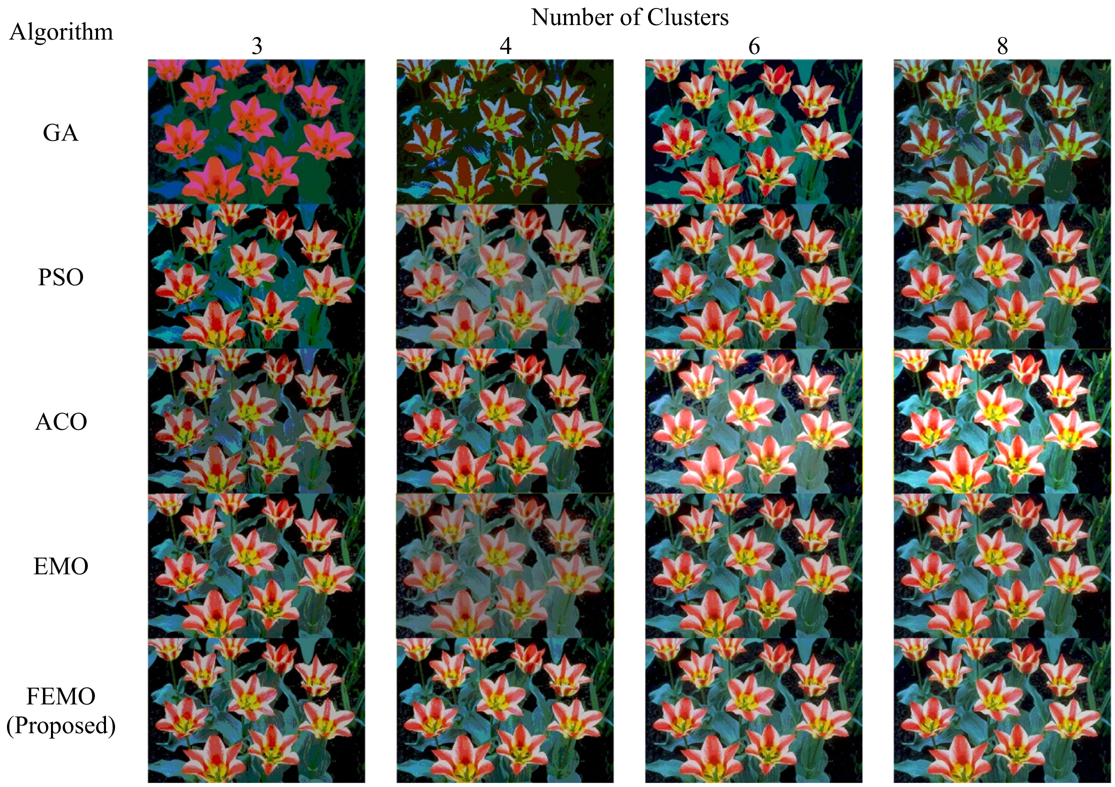

Fig. 18. Tulips image (color) (Fig. 4(n)-I_{014}) obtained using different methods and for different no. of clusters.

Table 3
Quantitative analysis and comparison of different algorithms using Davies–Bouldin index (the acceptable values are highlighted).

Image Id	Algorithm	No. of clusters			
		3	4	6	8
001	GA	**1.3914**	1.60013	1.7985	1.4193
	PSO	1.9666	**1.8196**	1.8225	1.9007
	ACO	1.4182	1.3256	**1.1093**	1.7155
	EMO	1.7419	1.6385	1.4755	**1.3027**
	FEMO (Proposed)	1.2748	1.3829	**0.9936**	1.1074
002	GA	**1.7845**	2.3639	2.1007	1.8674
	PSO	2.0361	**1.6784**	1.7102	1.6974
	ACO	2.6337	1.9637	1.9069	**1.8527**
	EMO	1.7843	1.7486	2.0374	**1.7109**
	FEMO (Proposed)	2.0396	**1.6801**	1.7023	1.9963
003	GA	1.9011	0.8693	**0.8687**	1.3329
	PSO	0.9368	**0.8875**	0.9963	1.2736
	ACO	1.4032	**1.1019**	1.2986	1.4378
	EMO	1.3019	**1.0014**	1.3960	1.0137
	FEMO (Proposed)	1.2013	**0.9963**	1.0113	0.9997
004	GA	2.0003	2.0416	**1.7485**	1.8639
	PSO	1.9015	1.7851	**1.6032**	1.7663
	ACO	1.8056	1.7741	**1.4398**	1.6327
	EMO	1.9306	**1.4916**	1.7480	1.8023
	FEMO (Proposed)	2.0136	1.4863	**1.3918**	1.6309
005	GA	1.9608	1.8867	**1.7486**	1.8817
	PSO	**1.8607**	1.9605	1.8863	1.9036
	ACO	1.9306	1.8990	**1.6031**	1.7448
	EMO	2.0003	2.0126	1.9306	**1.8803**
	FEMO (Proposed)	1.8805	1.6329	**1.5589**	1.7813
006	GA	0.9906	1.0325	**0.8923**	1.2036
	PSO	1.4205	1.3062	**1.0031**	2.0003
	ACO	0.9940	**0.8709**	1.0231	1.2031
	EMO	0.9756	0.9806	**0.8903**	1.0032
	FEMO (Proposed)	1.0596	0.7863	0.6696	1.4829

(continued on next page)

Table 3 (*continued*).

Image Id	Algorithm	No. of clusters			
		3	4	6	8
007	GA	1.8509	**1.6332**	1.9608	2.0037
	PSO	2.0369	**1.5026**	1.6478	1.9806
	ACO	1.9936	2.0019	**1.7206**	1.8476
	EMO	**1.2308**	1.8845	2.0063	2.0196
	FEMO (Proposed)	**1.1101**	1.8929	1.4063	1.7718
008	GA	2.8603	**2.3695**	2.9063	2.8693
	PSO	1.9963	1.8569	**1.4757**	1.7486
	ACO	1.8677	**1.5869**	1.8894	1.7728
	EMO	1.9698	1.5862	**1.4869**	1.4983
	FEMO (Proposed)	1.6689	1.7842	**1.3099**	1.9907
009	GA	1.9586	1.9086	**1.7774**	1.8693
	PSO	**1.3396**	2.1039	1.2019	2.0007
	ACO	**1.2096**	1.7059	1.8869	1.3692
	EMO	1.8692	1.7689	**1.2307**	1.8869
	FEMO (Proposed)	1.0112	1.4966	**1.3389**	1.8639
010	GA	2.4636	2.0456	**1.8459**	1.9963
	PSO	1.7863	**1.4905**	1.5369	1.7580
	ACO	2.0304	2.0036	**1.8075**	1.9063
	EMO	2.0366	**1.3027**	1.4058	1.7059
	FEMO (Proposed)	1.8968	**1.2309**	2.0193	1.9035
011	GA	**1.22558819**	2.59462352	2.89373473	2.299568245
	PSO	1.25500998	2.11313723	**1.23359842**	2.49479879
	ACO	**1.32574025**	2.00892876	1.9393609	2.705793997
	EMO	2.21537274	2.69433184	2.19383352	**2.065146191**
	FEMO (Proposed)	**1.02822943**	1.64498839	2.34796363	1.965189816
012	GA	2.2725938	2.44187343	3.06517091	**1.301301326**
	PSO	2.29770688	1.49987752	**1.13358178**	1.910599643
	ACO	1.86755074	2.95019591	1.43823012	**1.058889481**
	EMO	1.25763821	**1.22188233**	2.24624283	1.402418545
	FEMO (Proposed)	1.44713586	1.55978613	2.30040073	**1.003274389**
013	GA	2.1900947	1.88694452	**1.83113986**	2.414954615
	PSO	**1.01294032**	1.87395824	3.36971456	1.55023166
	ACO	**1.20563868**	2.04306534	1.77442626	1.205742313
	EMO	2.40456391	1.56893489	1.42894312	**1.248845498**
	FEMO (Proposed)	**1.06843376**	1.67982819	2.44082653	1.136159735
014	GA	**1.68170672**	1.72991509	1.94847257	1.864446787
	PSO	**1.31816188**	2.88317216	2.38730817	3.583518426
	ACO	**1.24863618**	1.68603603	2.14921125	2.340184428
	EMO	1.92768053	2.59176276	**1.78270533**	3.112499467
	FEMO (Proposed)	**1.41692409**	1.42988099	2.95098201	2.169210088
015	GA	**1.12332979**	1.59404807	1.81646097	1.316004409
	PSO	**1.87527306**	2.72972505	3.91408282	3.525843619
	ACO	**1.41262341**	3.02402041	3.85860157	3.049830964
	EMO	1.85498334	**1.22364678**	2.2340117	3.224871571
	FEMO (Proposed)	1.73621701	3.56498897	2.95795424	**1.203028635**
Average	GA	1.843694213	1.8665623	1.9468453	**1.833578**
	PSO	**1.66935947**	1.832738	1.7948124	2.0729861
	ACO	**1.62311928**	1.8630498	1.7896687	1.7895294
	EMO	1.766749249	**1.647744**	1.6995491	1.7918388
	FEMO (Proposed)	**1.45688934**	1.6165915	1.7600018	1.6003508

the biomedical image segmentation. Many clustering algorithms suffer from the initial selection of cluster centers. The proposed FEMO method computes the desired number of segments by randomly initializing the cluster centers and reaches the global optimum by optimizing the fuzzy objective function. The proposed method is tested and compared using four popular and frequently used cluster validity indices namely Davies–Bouldin index, Xie–Beni index, Dunn index, and index. The qualitative and quantitative analysis shows that the proposed FEMO method can determine the optimal cluster centers and can outperform some of the standard optimization algorithms. The proposed method is tested and compared for the different number of clusters to prove its efficiency and effectiveness. This approach can also be tested on different types of images with or without any modification. The promising results will certainly inspire other researchers to explore this domain and develop some sophisticated algorithms to enrich the field of computer vision. The proposed approach is already successfully demonstrated and applied to different types of biomedical images as well as on some of the standard test images. This approach is certainly useful for various real-life applications like extraction of the lung nodules, tumor identification, identification of different foreign bodies inside the body as well as inside cells, cell counting, continuous assessment of patients, easy interpretation of the biomedical images, quantification of the tissue volumes, designing of the treatment flow and many more.

8. Discussion and future scopes

The proposed approach produces promising segmentation outputs as well as better quantitative results. The overall average of all 15 images is appended at the bottom of each table to get an insight into the overall performance of the proposed system as well as the performance of the other systems. It can be

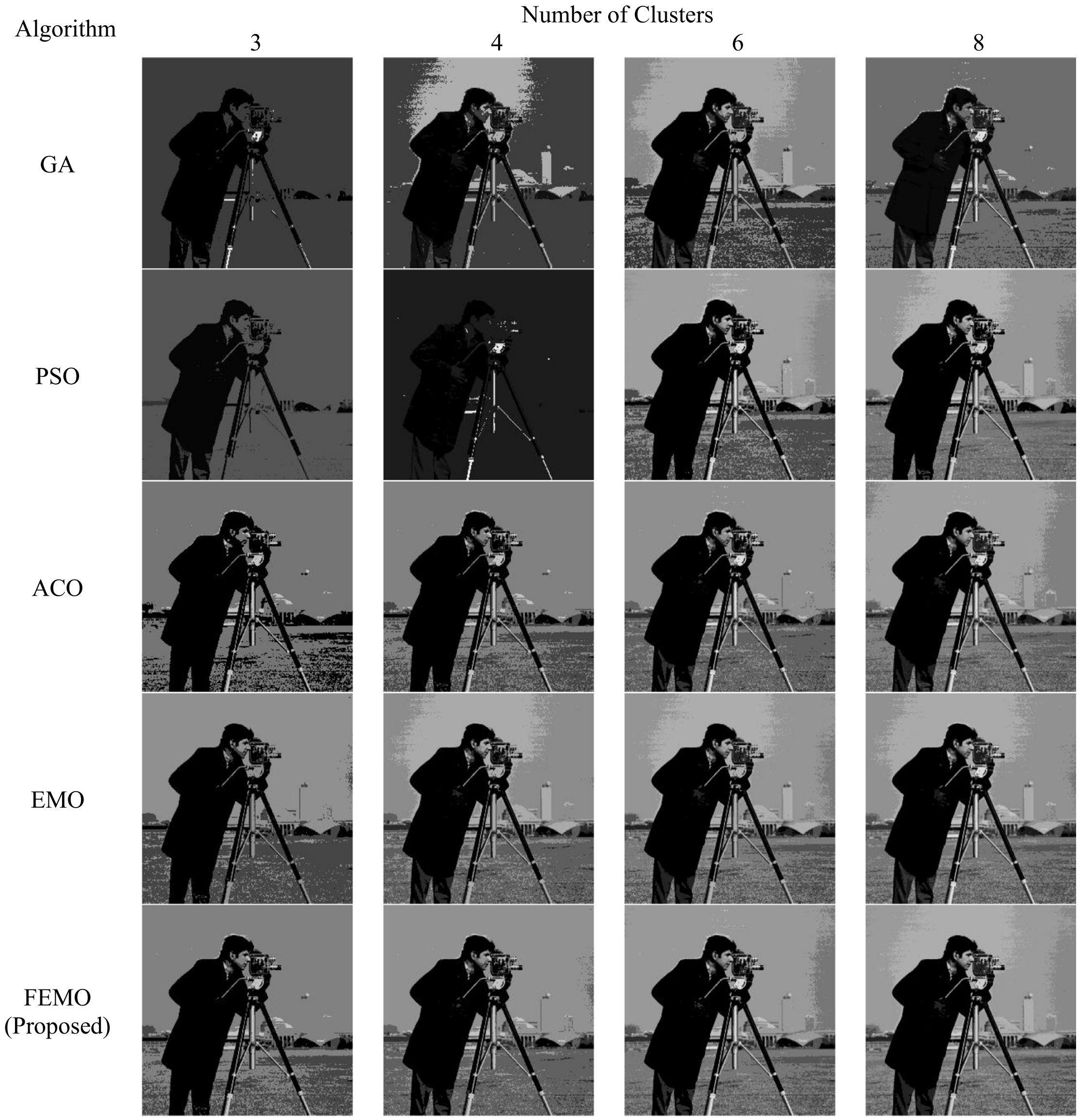

Fig. 19. Cameraman image (grayscale) (Fig. 4(o)-I_{015}) obtained using different methods and for different no. of clusters.

Table 4
Quantitative analysis and comparison of different algorithms using Xie–Beni index (the acceptable values are highlighted).

Image Id	Algorithm	No. of clusters			
		3	4	6	8
001	GA	1.9863	1.8637	**1.2569**	1.8963
	PSO	1.5967	1.7586	**1.4963**	1.5586
	ACO	**1.3266**	1.4586	1.3376	1.5278
	EMO	1.4386	1.5369	**1.3369**	1.4757
	FEMO (Proposed)	1.6348	1.1106	**1.1014**	1.3966
002	GA	2.6931	3.4415	2.3596	**2.1758**
	PSO	1.9986	2.3468	**1.5536**	2.0034
	ACO	2.3391	**2.0135**	2.3332	2.1903
	EMO	3.1963	2.0034	**1.9638**	2.1034
	FEMO (Proposed)	2.4537	1.9936	1.8837	2.2034
003	GA	4.1023	3.0069	**2.7362**	3.0344
	PSO	3.1692	3.9968	**2.4396**	2.4997
	ACO	3.9001	3.6832	3.4759	**2.8779**
	EMO	2.9047	2.9986	**2.6937**	2.7966
	FEMO (Proposed)	2.7968	2.8869	**2.4371**	2.5009

(*continued on next page*)

Table 4 (*continued*).

Image Id	Algorithm	No. of clusters			
		3	4	6	8
004	GA	1.9406	**1.6639**	2.0693	1.7586
	PSO	**2.0001**	2.1033	2.0236	2.1470
	ACO	2.3240	1.7685	**1.6641**	2.1333
	EMO	1.9341	**1.3358**	1.4769	1.8620
	FEMO (Proposed)	1.8346	**1.3341**	1.7935	1.6374
005	GA	2.0397	1.5860	**1.4963**	1.4995
	PSO	2.9638	**1.9348**	2.1142	2.0315
	ACO	3.6015	**1.7935**	2.4109	2.1113
	EMO	2.0936	1.4152	**1.3369**	1.5742
	FEMO (Proposed)	2.0037	1.3963	**1.2906**	1.5704
006	GA	1.7896	0.96386	**0.7596**	0.9968
	PSO	**0.8696**	0.9935	0.9856	1.6023
	ACO	0.9687	**0.7758**	1.2043	1.1123
	EMO	1.6356	**0.9968**	1.2034	0.9991
	FEMO (Proposed)	0.9346	**0.8106**	1.0032	1.3690
007	GA	2.9637	4.1153	**2.3476**	3.1026
	PSO	4.1906	3.0631	3.1333	**2.1936**
	ACO	3.4906	4.1023	2.9356	**2.4418**
	EMO	2.9354	4.1056	3.6639	**2.7748**
	FEMO (Proposed)	2.7053	2.9936	2.7418	**2.7610**
008	GA	1.9346	2.0013	**1.4865**	1.8023
	PSO	**1.4963**	1.6359	2.0136	1.5563
	ACO	1.7058	1.6302	**1.5539**	1.8063
	EMO	2.0316	1.7569	**1.6953**	1.7638
	FEMO (Proposed)	2.0031	**1.3032**	1.7266	1.8996
009	GA	**0.9963**	1.0136	1.3363	1.5234
	PSO	3.0263	1.9696	**1.7459**	2.0364
	ACO	**1.5031**	2.5569	1.6324	1.9185
	EMO	1.4023	**1.2236**	1.4126	1.3312
	FEMO (Proposed)	**1.0126**	1.1309	1.3966	1.2033
010	GA	**1.0396**	1.2306	1.1036	1.5036
	PSO	1.9635	2.1136	**1.2365**	1.4453
	ACO	3.1063	2.1965	**2.1103**	2.9635
	EMO	1.4392	2.1003	**1.1386**	2.3369
	FEMO (Proposed)	1.8829	1.2306	**1.0014**	2.0936
011	GA	**1.55622979**	3.29764373	1.9111625	2.1846914
	PSO	**1.26123057**	1.33139084	2.6753039	2.666595764
	ACO	1.38685565	**1.09618808**	2.03975854	2.716090062
	EMO	2.18882254	2.99244763	2.35267781	**1.8237221**
	FEMO (Proposed)	1.43199184	**1.08863333**	2.23279981	2.07815449
012	GA	**1.55855226**	1.6449514	2.58197214	1.917271771
	PSO	2.60844917	2.0919962	2.54501909	**2.032380406**
	ACO	**1.09378924**	2.26391146	2.07872967	2.249244762
	EMO	**1.21586022**	1.9493223	2.25589934	1.60497401
	FEMO (Proposed)	**1.07075991**	1.63965413	1.49352536	1.672938003
013	GA	2.17231151	**1.85756078**	1.99809302	1.879338692
	PSO	**1.46494438**	1.48581065	1.95055008	1.526163783
	ACO	1.83618104	2.22312739	2.06642438	**1.800932299**
	EMO	1.70541929	**1.25225462**	1.78713725	1.672753844
	FEMO (Proposed)	**1.0035261**	1.13095041	1.61364378	1.909368202
014	GA	1.21610426	1.04945022	1.4152948	**1.006502634**
	PSO	**1.76952746**	3.23737406	2.75619659	3.474456412
	ACO	2.45396235	2.63888169	**2.29780847**	2.398212991
	EMO	2.81408457	**1.71506566**	2.77900911	2.129794147
	FEMO (Proposed)	**1.01508116**	2.06480047	2.36401478	2.268506669
015	GA	1.00693288	2.43229358	**1.00053328**	2.149544424
	PSO	**1.81179581**	3.15038303	3.61384502	3.422623424
	ACO	2.06625074	**1.67891175**	3.46823612	2.720478278
	EMO	**2.17866432**	2.75567202	2.76789092	2.756816405
	FEMO (Proposed)	1.21971159	2.10878281	1.41636644	**1.008487255**
Average	GA	1.933062	2.077904	**1.72393**	1.8953766
	PSO	**2.146043**	2.214197	2.1522076	2.1464213
	ACO	2.2068559	**2.125335**	2.1739438	2.1978639
	EMO	2.0742834	2.0091908	1.9909743	**1.933717**
	FEMO (Proposed)	1.666878	**1.614881**	1.69975	1.838177

observed that in most situations the proposed method achieves the optimum values of the different indices. Also, the proposed approach shows a good convergence property with the Davies–Bouldin index. In this work, four different quantitative metrics are used among which Davies–Bouldin and Xie–Beni indices are expected to be minimized whereas Dunn and indices are expected to be maximized. The convergence curves are plotted against the Davies–Bouldin index. Typically, the biomedical

Table 5
Quantitative analysis and comparison of different algorithms using Dunn index (the acceptable values are highlighted).

Image Id	Algorithm	No. of clusters			
		3	4	6	8
001	GA	2.10684432	2.6323655	**3.94267343**	2.750469528
	PSO	4.09737274	**4.61776236**	3.41793133	3.954059609
	ACO	**4.18330134**	2.03158805	3.14949074	2.990604363
	EMO	2.94411463	**3.63319761**	2.52039526	3.101683204
	FEMO (Proposed)	1.62773772	**3.9289514**	2.03019678	1.645795109
002	GA	0.2677365	1.18561022	**1.29520824**	0.789756387
	PSO	1.35437746	0.54892247	**1.87736709**	1.500374186
	ACO	0.64290405	1.03601871	0.58525336	**1.129794743**
	EMO	0.8412856	1.31481202	1.02664008	**1.776730354**
	FEMO (Proposed)	1.21635105	1.93850459	**2.97235228**	1.454539325
003	GA	0.59273528	**1.60429692**	1.48739178	1.334418863
	PSO	0.72222556	1.24179033	**1.93278002**	1.597345801
	ACO	0.7340354	1.28633087	**2.00589544**	0.599778728
	EMO	1.7451169	1.29041	1.77961243	**1.895297768**
	FEMO (Proposed)	1.79089115	1.0294552	**2.4596622**	2.127554341
004	GA	0.32102814	1.05214265	**1.33044828**	0.371470931
	PSO	0.64810528	1.16054222	1.27972472	**2.290537366**
	ACO	0.94482689	0.25774691	**1.1088511**	0.433515732
	EMO	1.30996974	1.44911615	**2.05141066**	1.906672612
	FEMO (Proposed)	**1.89290717**	1.73391237	1.68078375	1.452485367
005	GA	0.99832645	1.31626032	0.32888882	**1.435277616**
	PSO	0.54103151	0.36737209	0.89499168	**1.17794893**
	ACO	0.92769763	1.10584821	1.39791205	**2.211863428**
	EMO	2.1750528	1.85130601	**2.23116263**	1.827804988
	FEMO (Proposed)	**2.6822522**	1.25468148	1.88162193	1.445491066
006	GA	0.92588466	1.62992615	**1.89835684**	1.687126037
	PSO	0.09380177	**2.41009495**	2.33846089	1.50938601
	ACO	2.60217521	2.14495306	2.04661697	**3.068051399**
	EMO	2.25291123	1.16413986	2.38094198	**2.934582592**
	FEMO (Proposed)	1.04263556	1.1997414	**2.9960215**	1.879118982
007	GA	0.24880845	0.15641318	**1.83312536**	1.68204198
	PSO	2.45043209	1.3119737	**2.93396522**	1.472468457
	ACO	0.14673109	1.24088346	**1.38335208**	0.4151167
	EMO	0.57306333	1.27673303	1.35764736	**1.510730711**
	FEMO (Proposed)	2.0857256	2.32490087	1.66463447	**3.471056388**
008	GA	0.74537946	1.5014925	0.34921433	**1.6932563**
	PSO	**2.20041125**	1.05124401	1.50087055	1.188172988
	ACO	0.23697646	0.79843611	**0.90101582**	0.32844596
	EMO	0.98104075	0.2860457	0.15645806	**1.222877794**
	FEMO (Proposed)	2.13070338	**2.71004601**	1.30759081	1.049505722
009	GA	0.15338042	0.62231323	0.1779328	**1.078005899**
	PSO	**3.51732955**	2.52062826	1.7442897	0.899026538
	ACO	1.74127656	2.90424488	**3.18302024**	2.434732611
	EMO	3.98545719	2.98710736	2.83809278	**4.386954649**
	FEMO (Proposed)	2.32416059	**4.21443569**	2.76832288	2.151602797
010	GA	1.78282187	**4.32602689**	1.06990152	2.465687336
	PSO	**1.71737858**	1.44268825	1.21172858	1.303959771
	ACO	**2.25435492**	0.78567359	1.4968575	1.530707916
	EMO	1.66031439	1.17950249	**2.52249316**	1.974179378
	FEMO (Proposed)	2.01080214	3.67237271	**4.17804411**	3.606283668
011	GA	0.55622979	**3.29764373**	1.48111625	2.1846914
	PSO	1.26123057	1.33139084	**2.6753039**	2.666595764
	ACO	1.38685565	1.00618808	2.03975854	**2.716090062**
	EMO	2.18882254	**2.99244763**	2.35267781	1.8237221
	FEMO (Proposed)	1.43199184	3.28863333	2.23279981	**3.47815449**
012	GA	1.55855226	1.6449514	**2.58197214**	1.917271771
	PSO	**2.60844917**	2.0919962	2.54501909	2.032380406
	ACO	1.03378924	**2.26391146**	2.07872967	2.249244762
	EMO	1.21586022	1.9493223	**2.25589934**	1.60497401
	FEMO (Proposed)	1.47075991	2.63965413	**2.99352536**	1.672938003
013	GA	**2.17231151**	1.85756078	1.99809302	1.879338692
	PSO	0.46494438	1.48581065	**1.95055008**	1.526163783
	ACO	1.83618104	**2.22312739**	2.06642438	0.870932299
	EMO	1.70541929	1.25225462	**1.78713725**	1.672753844
	FEMO (Proposed)	1.23335261	2.13095041	**2.61364378**	1.909368202

(*continued on next page*)

images contain different regions which are not properly differentiable and contain uncertainties. It is essential to design a sophisticated approach that can effectively model such as uncertainties and subjectivity. The proposed fuzzy EMO approach

Table 5 (*continued*).

Image Id	Algorithm	No. of clusters			
		3	4	6	8
014	GA	1.21610426	1.04945022	**1.4152948**	0.886502634
	PSO	1.76952746	3.23737406	2.75619659	**3.474456412**
	ACO	2.45396235	**2.63888169**	2.29780847	2.398212991
	EMO	**2.81408457**	1.71506566	2.77900911	2.129794147
	FEMO (Proposed)	1.01508116	2.06480047	**2.36401478**	2.268506669
015	GA	0.80693288	**2.93229358**	2.69453328	2.149544424
	PSO	1.81179581	3.15038303	**3.61384502**	3.422623424
	ACO	2.06625074	1.67891175	**3.46823612**	2.720478278
	EMO	2.17866432	2.75567202	**2.76789092**	2.756816405
	FEMO (Proposed)	3.21971159	**4.10878281**	2.41636644	2.208487255
Average	GA	0.9635384	**1.78725**	1.5922767	1.620324
	PSO	1.6838942	1.8646649	**2.178202**	2.0010333
	ACO	1.5460879	1.5601829	**1.947281**	1.739838
	EMO	1.9047452	1.8064755	2.0538313	**2.168372**
	FEMO (Proposed)	1.8116709	**2.549322**	2.4373054	2.1213925

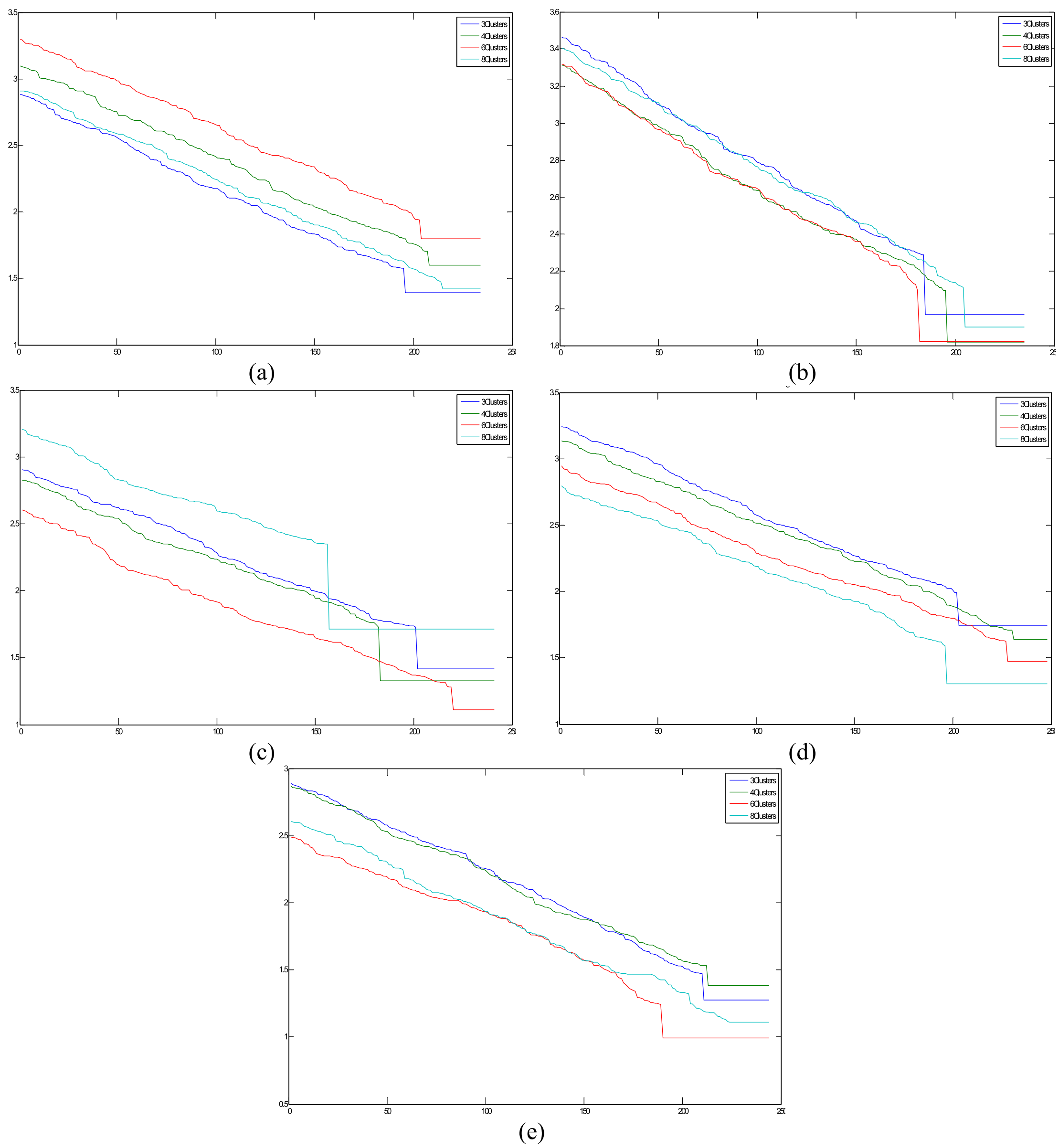

Fig. 20. Comparison of the convergence curves which are obtained using different methods and for the different number of clusters. The Davies–Bouldin index for the image I_{001} is plotted in the Y-axis and the number of iterations is plotted in the X-axis of each curve. (a) Genetic Algorithm, (b) PSO, (c) ACO, (d) EMO, (e) FEMO (proposed).

Table 6
Quantitative analysis and comparison of different algorithms using β index (the acceptable values are highlighted).

Image Id	Algorithm	No. of clusters			
		3	4	6	8
001	GA	0.91524179	**2.74207958**	2.35857016	2.436514439
	PSO	0.90593466	1.49106811	2.70495877	**2.809175242**
	ACO	1.47670969	1.07893198	1.37159153	**2.812117977**
	EMO	**2.82095422**	2.50559793	1.66338994	2.430408505
	FEMO (Proposed)	1.52238599	1.47360149	**2.99580808**	1.940634159
002	GA	1.09855016	**2.72771622**	2.4897761	0.922036474
	PSO	**2.47122669**	1.65672704	1.56352774	1.947174303
	ACO	0.44665583	2.51892634	1.72710177	**2.803523495**
	EMO	1.45500991	**2.49434297**	1.73852224	1.98205397
	FEMO (Proposed)	1.53693387	1.03087517	1.808699	**2.942807502**
003	GA	1.52168335	1.51061638	1.82985963	**2.088872941**
	PSO	1.41631418	2.06018156	**2.28090855**	1.867930506
	ACO	1.18980896	1.40091213	1.26245703	**1.753314506**
	EMO	**2.20409159**	1.40843568	1.95677806	2.100433926
	FEMO (Proposed)	0.69408921	**2.34753699**	2.04171088	1.225044971
004	GA	0.33698412	1.42479306	**1.83198787**	1.730993506
	PSO	1.17578502	2.2921571	**2.70095776**	2.601018679
	ACO	2.65091089	2.61030674	**2.67884316**	2.226518542
	EMO	1.50526967	**2.24741154**	2.0457924	1.480549377
	FEMO (Proposed)	1.08031794	2.07185063	**3.17901003**	2.08012608
005	GA	0.91867046	1.37766102	1.73546544	**1.766758803**
	PSO	2.72940603	3.36733356	**3.78709975**	2.1958566
	ACO	2.33985503	2.35153902	**3.08448193**	2.633749867
	EMO	1.98063279	2.25302953	2.93141651	**3.489155257**
	FEMO (Proposed)	2.38600413	**4.17570849**	2.81978148	2.06853741
006	GA	1.78973213	**2.24190171**	1.60745351	2.032131432
	PSO	1.59798727	1.65681247	2.11539422	**2.232563412**
	ACO	1.46818218	1.21504014	2.85141786	**3.334774179**
	EMO	2.19953941	2.4524239	2.85575533	**2.887327065**
	FEMO (Proposed)	1.28657943	2.2363775	**3.69235086**	1.929884338
007	GA	1.54918912	1.10749895	1.5136247	**2.097119778**
	PSO	1.90683966	2.43227058	**3.77514388**	2.905601727
	ACO	1.10112824	2.19953058	**2.76489802**	0.918605359
	EMO	**3.24535456**	2.817846	2.77764267	1.921654463
	FEMO (Proposed)	1.7773547	**3.78376071**	1.75235784	2.738132739
008	GA	2.29873351	**3.12706495**	2.69125105	1.775482067
	PSO	1.01198481	**1.83028036**	1.30190189	1.584473741
	ACO	1.92403152	1.9856319	**2.88560901**	2.181791753
	EMO	2.1904004	**3.95781391**	3.29304085	3.642363233
	FEMO (Proposed)	2.30398648	**4.51267398**	2.36726003	2.316322133
009	GA	0.78766122	1.45709035	2.19703267	**3.375535468**
	PSO	**2.96532012**	1.25859332	2.44028153	2.098095486
	ACO	1.7513011	2.46368249	**3.1290367**	1.730897185
	EMO	2.33220304	1.98146907	2.80564307	**2.920692368**
	FEMO (Proposed)	1.33097573	2.07303108	**3.91531093**	2.86103792
010	GA	2.80969578	**3.25400478**	2.68280203	2.796858331
	PSO	**3.00298009**	3.37861394	3.82941452	3.020424656
	ACO	1.76621804	1.21036025	**2.44638482**	2.422413256
	EMO	2.92081599	2.52073724	**3.30579962**	2.451372497
	FEMO (Proposed)	**3.16446397**	2.08222681	2.67426106	1.947756794
011	GA	1.22596717	2.24990053	**2.53158683**	2.197758586
	PSO	0.83293028	1.60889133	1.7629218	**2.057221716**
	ACO	1.54943491	0.78249959	1.72345116	**2.491332718**
	EMO	1.99816884	**3.83867559**	2.23004864	2.781444522
	FEMO (Proposed)	2.06798976	**2.1419901**	2.11940829	2.004780002
012	GA	**2.11798834**	1.36478426	2.03463558	1.911906078
	PSO	1.9808905	**2.84320719**	2.42233426	2.427752219
	ACO	1.0597706	1.80922994	0.9574932	**2.357979296**
	EMO	1.98444106	1.36481281	**2.48239255**	2.427419411
	FEMO (Proposed)	0.99556503	0.61196515	**2.40265821**	1.432376661
013	GA	1.44033882	2.14848884	**2.65316556**	1.243763253
	PSO	0.8580722	2.55693102	**2.93476096**	2.802187973
	ACO	**1.8518455**	1.60883885	1.7927086	1.649166282
	EMO	1.62611906	1.5938718	1.22158014	**2.3445054**
	FEMO (Proposed)	0.79865138	1.89075923	**2.84599887**	1.612150642

(*continued on next page*)

can effectively handle this problem and the local and the global search helps to explore the total solution space efficiently and hence the proposed approach is performing well compared to the other of its competitors.

Table 6 (*continued*).

Image Id	Algorithm	No. of clusters			
		3	4	6	8
014	GA	1.39947278	1.2816079	**1.64938225**	1.305378665
	PSO	1.14851482	2.71307196	2.07346558	**2.986644195**
	ACO	2.20885226	2.25931047	**3.44954624**	2.532889974
	EMO	2.13324824	2.00801094	1.71617097	**2.270355367**
	FEMO (Proposed)	1.21266947	2.22675242	2.41003872	**2.503656749**
015	GA	1.3290628	1.91381348	2.86268103	**2.355607465**
	PSO	2.08988922	3.88624304	**4.22186428**	3.206249336
	ACO	2.17439047	2.50084122	3.54918153	**3.794969323**
	EMO	2.41241672	2.86172074	2.73138504	**3.854191604**
	FEMO (Proposed)	3.40080229	**3.79063462**	3.9564049	1.805177409
Average	GA	1.4359314	1.9952681	**2.177952**	2.0024478
	PSO	1.739605	2.3354922	**2.660996**	2.4494913
	ACO	1.6639397	1.8663721	**2.37828**	2.3762696
	EMO	2.2005777	2.4204133	2.3836905	**2.598928**
	FEMO (Proposed)	1.703918	2.429983	**2.732071**	2.093895

The local search method in the EMO can also be replaced by other methods. In fact, in some works, the local search method is replaced by other algorithms (e.g. genetic algorithm). In this work, only the original method is considered because the proposed FEMO method is designed to incorporate the type 2 fuzzy system in the actual EMO method and this blend is used in the biomedical image segmentation. So, the effect of the modifications in the local search method in the FEMO algorithm can also be explored next. The step length for the movement of the particles is computed with a randomly generated value ε which belongs uniformly in the range 0 and 1 (refer Eq. (11)). Now, this step length can be replaced with some other distribution and the performance can be checked. From algorithm 6, it can be observed that there is no need to move the point with the best fitness value ζ^{best} and therefore, the force exerted on this point is no longer needed to be computed.

CRediT authorship contribution statement

Shouvik Chakraborty: Solution formulation, Conceptualization, Methodology, Software development, Article writing, Editing, investigation. **Kalyani Mali:** Formal analysis, Resources, review, supervision.

Declaration of competing interest

The authors declare that they have no known competing financial interests or personal relationships that could have appeared to influence the work reported in this paper.

Acknowledgments

The authors would like to express their gratitude and thank the editors, anonymous reviewers, and referees for their valuable comments and suggestions which are helpful in further improvement of this research work.

References

[1] N. Dhanachandra, Y.J. Chanu, An image segmentation approach based on fuzzy c-means and dynamic particle swarm optimization algorithm, Multimedia Tools Appl. (2020) 1–20, http://dx.doi.org/10.1007/s11042-020-08699-8.

[2] S. Chakraborty, S. Chatterjee, A.S. Ashour, K. Mali, N. Dey, Intelligent computing in medical imaging: A study, in: N. Dey (Ed.), Adv. Appl. Metaheuristic Comput., IGI Global, 2017, pp. 143–163, http://dx.doi.org/10.4018/978-1-5225-4151-6.ch006.

[3] S. Hore, S. Chakraborty, S. Chatterjee, N. Dey, A.S. Ashour, L. Van Chung, G. Nguyen, D.-. Nhuong Le, An integrated interactive technique for image segmentation using stack based seeded region growing and thresholding, Int. J. Electr. Comput. Eng. 6 (2016) 2773–2780, http://dx.doi.org/10.11591/ijece.v6i6.11801.

[4] S. Hore, S. Chakroborty, A.S. Ashour, N. Dey, A.S. Ashour, D. Sifaki-Pistolla, T. Bhattacharya, S.R.B. Chaudhuri, Finding contours of hippocampus brain cell using microscopic image analysis, J. Adv. Microsc. Res. 10 (2015) 93–103, http://dx.doi.org/10.1166/jamr.2015.1245.

[5] S. Chakraborty, S. Chatterjee, N. Dey, A.S. Ashour, A.S. Ashour, F. Shi, K. Mali, Modified cuckoo search algorithm in microscopic image segmentation of hippocampus, Microsc. Res. Tech. (2017) 1–22, http://dx.doi.org/10.1002/jemt.22900.

[6] S. Chakraborty, K. Mali, An overview of biomedical image analysis from the deep learning perspective, in: S. Chakraborty, K. Mali (Eds.), Appl. Adv. Mach. Intell. Comput. Vis. Object Recognit. Emerg. Res. Oppor., IGI Global, 2020, http://dx.doi.org/10.4018/978-1-7998-2736-8.ch008.

[7] K.S. Chuang, H.L. Tzeng, S. Chen, J. Wu, T.J. Chen, Fuzzy c-means clustering with spatial information for image segmentation, Comput. Med. Imaging Graph. 30 (2006) 9–15, http://dx.doi.org/10.1016/j.compmedimag.2005.10.001.

[8] S.K. Choy, K. Yuen, C. Yu, Fuzzy bit-plane-dependence image segmentation, Signal Process. 154 (2019) 30–44, http://dx.doi.org/10.1016/j.sigpro.2018.08.010.

[9] S. Chakraborty, A. Raman, S. Sen, K. Mali, S. Chatterjee, H. Hachimi, Contrast optimization using elitist metaheuristic optimization and gradient approximation for biomedical image enhancement, in: 2019 Amity Int. Conf. Artif. Intell., IEEE, 2019, pp. 712–717, http://dx.doi.org/10.1109/AICAI.2019.8701367.

[10] S. Chakraborty, K. Mali, S. Chatterjee, S. Banerjee, A. Sah, S. Pathak, S. Nath, D. Roy, Bio-medical image enhancement using hybrid metaheuristic coupled soft computing tools, in: 2017 IEEE 8th Annu. Ubiquitous Comput. Electron. Mob. Commun. Conf. UEMCON 2017, 2018, http://dx.doi.org/10.1109/UEMCON.2017.8249036.

[11] L.a. Zadeh, Fuzzy sets, Inf. Control 8 (1965) 338–353, http://dx.doi.org/10.1016/S0019-9958(65)90241-X.

[12] X. Lei, H. Ouyang, Image segmentation algorithm based on improved fuzzy clustering, Cluster Comput. 22 (2019) 13911–13921, http://dx.doi.org/10.1007/s10586-018-2128-9.

[13] M. Zhang, W. Jiang, X. Zhou, Y. Xue, S. Chen, A hybrid biogeography-based optimization and fuzzy C-means algorithm for image segmentation, Soft Comput. 23 (2019) 2033–2046, http://dx.doi.org/10.1007/s00500-017-2916-9.

[14] Y. a Tolias, S.M. Panas, Image segmentation by a fuzzy clustering algorithm using adaptive spatially constrained membership functions, IEEE Trans. Syst. Man Cybern. A 28 (1998) 359–369, http://dx.doi.org/10.1109/3468.668967.

[15] J.C. Bezdek, R. Ehrlich, W. Full, FCM: The fuzzy c-means clustering algorithm, Comput. Geosci. 10 (1984) 191–203, http://dx.doi.org/10.1016/0098-3004(84)90020-7.

[16] O. Castillo, P. Melin, J. Kacprzyk, W. Pedrycz, Type-2 Fuzzy Logic: Theory and Applications, Institute of Electrical and Electronics Engineers (IEEE), 2008, p. 145, http://dx.doi.org/10.1109/grc.2007.118.

[17] E. Cuevas, D. Oliva, M. Díaz, D. Zaldivar, M. Pérez-Cisneros, G. Pajares, White blood cell segmentation by circle detection using electromagnetism-like optimization, Comput. Math. Methods Med. 2013 (2013) 395071, http://dx.doi.org/10.1155/2013/395071.

[18] C.H. Lee, C.T. Li, F.Y. Chang, A species-based improved electromagnetism-like mechanism algorithm for TSK-type interval-valued neural fuzzy system optimization, Fuzzy Sets and Systems 171 (2011) 22–43, http://dx.doi.org/10.1016/j.fss.2011.02.004.

[19] D. Debels, M. Vanhoucke, The electromagnetism meta-heuristic applied to the resource-constrained project scheduling problem, in: Lect. Notes

Comput. Sci. (Including Subser. Lect. Notes Artif. Intell. Lect. Notes Bioinformatics), Springer, Berlin, Heidelberg, 2006, pp. 259–270, http://dx.doi.org/10.1007/11740698_23.
[20] A.M.A.C. Rocha, E.M.G.P. Fernandes, Implementation of the electromagnetism-like algorithm with a constraint-handling technique for engineering optimization problems, in: Proc. - 8th Int. Conf. Hybrid Intell. Syst. HIS 2008, 2008, pp. 690–695, http://dx.doi.org/10.1109/HIS.2008.145.
[21] Q.H. Wang, J.C. Zeng, A new electromagnetism-like algorithm with chaos optimization, in: Proc. - Int. Conf. Comput. Asp. Soc. Networks, CASoN'10, 2010, pp. 535–538, http://dx.doi.org/10.1109/CASoN.2010.124.
[22] R. Dutta, R. Ganguli, V. Mani, Exploring isospectral cantilever beams using electromagnetism inspired optimization technique, Swarm Evol. Comput. 9 (2013) 37–46, http://dx.doi.org/10.1016/j.swevo.2012.09.005.
[23] C.H. Lee, F.K. Chang, Fractional-order PID controller optimization via improved electromagnetism-like algorithm, Expert Syst. Appl. 37 (2010) 8871–8878, http://dx.doi.org/10.1016/j.eswa.2010.06.009.
[24] N. Javadian, M. Gol Alikhani, R. Tavakkoli-Moghaddam, A discrete binary version of the electromagnetism-like heuristic for solving traveling salesman problem, in: Lect. Notes Comput. Sci. (Including Subser. Lect. Notes Artif. Intell. Lect. Notes Bioinformatics), Springer, Berlin, Heidelberg, 2008, pp. 123–130, http://dx.doi.org/10.1007/978-3-540-85984-0_16.
[25] H.R.E.-H. Bouchekara, Electromagnetic device optimization based on electromagnetism-like mechanism, 2013.
[26] C.T. Su, H.C. Lin, Applying electromagnetism-like mechanism for feature selection, Inf. Sci. (Ny) 181 (2011) 972–986, http://dx.doi.org/10.1016/j.ins.2010.11.008.
[27] C.S. Tsou, C.H. Kao, An electromagnetism-like meta-heuristic for multi-objective optimization, in: 2006 IEEE Congr. Evol. Comput. CEC 2006, 2006, pp. 1172–1178, http://dx.doi.org/10.1109/cec.2006.1688442.
[28] L. Pratiwi, Y.-H. Choo, A.K. Muda, N.A. Muda, Immune ant swarm optimization for optimum rough reducts generation, Int. J. Hybrid Intell. Syst. 10 (2016) 93–105, http://dx.doi.org/10.3233/his-130168.
[29] R.E. Precup, E.I. Voisan, E.M. Petriu, M.L. Tomescu, R.C. David, A.I. Szedlak-Stinean, R.C. Roman, Grey wolf optimizer-based approaches to path planning and fuzzy logic-based tracking control for mobile robots, Int. J. Comput. Commun. Control 15 (2020) 15, http://dx.doi.org/10.15837/IJCCC.2020.3.3844.
[30] Ş.I. Birbil, S.C. Fang, An electromagnetism-like mechanism for global optimization, J. Global Optim. 25 (2003) 263–282, http://dx.doi.org/10.1023/A:1022452626305.
[31] D. Oliva, E. Cuevas, G. Pajares, D. Zaldivar, V. Osuna, A multilevel thresholding algorithm using electromagnetism optimization, Neurocomputing 139 (2014) 357–381, http://dx.doi.org/10.1016/j.neucom.2014.02.020.
[32] F. Archetti, A. Candelieri, From Global Optimization to Optimal Learning, Springer, Cham, 2019, pp. 19–35, http://dx.doi.org/10.1007/978-3-030-24494-1_2.
[33] D.F. Yates, A.B. Templeman, T.B. Boffey, The complexity of procedures for determining minimum weight trusses with discrete member sizes, Int. J. Solids Struct. 18 (1982) 487–495, http://dx.doi.org/10.1016/0020-7683(82)90065-8.
[34] W.H. Tong, G.R. Liu, Optimization procedure for truss structures with discrete design variables and dynamic constraints, Comput. Struct. 79 (2001) 155–162, http://dx.doi.org/10.1016/S0045-7949(00)00124-3.
[35] K.J. Wang, A.M. Adrian, K.H. Chen, K.M. Wang, An improved electromagnetism-like mechanism algorithm and its application to the prediction of diabetes mellitus, J. Biomed. Inform. 54 (2015) 220–229, http://dx.doi.org/10.1016/j.jbi.2015.02.001.
[36] S. Chakraborty, S. Bhowmik, Blending roulette wheel selection with simulated annealing for job shop scheduling problem, in: IET Conf. Publ., 2015, http://dx.doi.org/10.1049/cp.2015.1696.
[37] S. Chakraborty, A. Seal, M. Roy, An elitist model for obtaining alignment of multiple sequences using genetic algorithm, in: 2nd Natl. Conf. NCETAS 2015, International Journal of Innovative Research in Science, Engineering and Technology, 2015, pp. 61–67.
[38] C. Blum, J. Puchinger, G.R. Raidl, A. Roli, Hybrid metaheuristics in combinatorial optimization: A survey, Appl. Soft Comput. J. 11 (2011) 4135–4151, http://dx.doi.org/10.1016/j.asoc.2011.02.032.
[39] S. Mahdavi, M.E. Shiri, S. Rahnamayan, Metaheuristics in large-scale global continues optimization: A survey, Inf. Sci. (Ny) 295 (2015) 407–428, http://dx.doi.org/10.1016/j.ins.2014.10.042.
[40] L. Bianchi, M. Dorigo, L.M. Gambardella, W.J. Gutjahr, A survey on metaheuristics for stochastic combinatorial optimization, Nat. Comput. 8 (2009) 239–287, http://dx.doi.org/10.1007/s11047-008-9098-4.
[41] S.J. Nanda, G. Panda, A survey on nature inspired metaheuristic algorithms for partitional clustering, Swarm Evol. Comput. 16 (2014) 1–18, http://dx.doi.org/10.1016/j.swevo.2013.11.003.
[42] I. Boussaïd, J. Lepagnot, P. Siarry, A survey on optimization metaheuristics, in: Inf. Sci. (Ny), Elsevier, 2013, pp. 82–117, http://dx.doi.org/10.1016/j.ins.2013.02.041.
[43] S. Chakraborty, K. Mali, Application of multiobjective optimization techniques in biomedical image segmentation—A study, in: Multi-Objective Optim., Springer Singapore, Singapore, 2018, pp. 181–194, http://dx.doi.org/10.1007/978-981-13-1471-1_8.
[44] M. Haseyama, M. Kumagai, H. Kitajima, Genetic algorithm based image segmentation for image analysis, in: ICASSP, IEEE Int. Conf. Acoust. Speech Signal Process. - Proc. Vol. 6, 1999, pp. 3445–3448, http://dx.doi.org/10.1109/icassp.1999.757583.
[45] L. Hongpo, S. Jun, W. Hai, T. Shuhua, T. Zhiguo, High resolution sonar image segmentation by PSO based fuzzy cluster method, in: Proc. - 4th Int. Conf. Genet. Evol. Comput. ICGEC 2010, 2010, pp. 18–21, http://dx.doi.org/10.1109/ICGEC.2010.13.
[46] Xiao-Nian Wang, Yuan-Jing Feng, Zu-Ren Feng, Ant colony optimization for image segmentation, in: 2005 Int. Conf. Mach. Learn. Cybern., Vol. 9, IEEE, 2005, pp. 5355–5360, http://dx.doi.org/10.1109/ICMLC.2005.1527890.
[47] S. Chakraborty, S. Bhowmik, Blending roulette wheel selection with simulated annealing for job shop scheduling problem, in: Michael Faraday IET Int. Summit 2015, Institution of Engineering and Technology, 2015, p. 100 (7.), http://dx.doi.org/10.1049/cp.2015.1696.
[48] I. Tsamardinos, L.E. Brown, C.F. Aliferis, The max–min hill-climbing Bayesian network structure learning algorithm, Mach. Learn. 65 (2006) 31–78, http://dx.doi.org/10.1007/s10994-006-6889-7.
[49] S. ichi Amari, Backpropagation and stochastic gradient descent method, Neurocomputing 5 (1993) 185–196, http://dx.doi.org/10.1016/0925-2312(93)90006-O.
[50] F.A. Lindholm, J.G. Fossum, E.L. Burgess, Application of the superposition principle to solar-cell analysis, IEEE Trans. Electron Devices 26 (1979) 165–171, http://dx.doi.org/10.1109/T-ED.1979.19400.
[51] M.P. Windham, Cluster validity for the fuzzy c-means clustering algorithm, IEEE Trans. Pattern Anal. Mach. Intell. PAMI-4 (1982) 357–363, http://dx.doi.org/10.1109/TPAMI.1982.4767266.
[52] R. Krishnapuram, J.M. Keller, A possibilistic approach to clustering, IEEE Trans. Fuzzy Syst. 1 (1993) 98–110, http://dx.doi.org/10.1109/91.227387.
[53] P. Melin, O. Mendoza, O. Castillo, An improved method for edge detection based on interval type-2 fuzzy logic, Expert Syst. Appl. 37 (2010) 8527–8535, http://dx.doi.org/10.1016/j.eswa.2010.05.023.
[54] F.C.H. Rhee, Uncertain fuzzy clustering: Insights and recommendations, IEEE Comput. Intell. Mag. 2 (2007) 44–56, http://dx.doi.org/10.1109/MCI.2007.357193.
[55] F.C.H. Rhee, Cheul Hwang, A type-2 fuzzy C-means clustering algorithm, in: Proc. Jt. 9th IFSA World Congr. 20th NAFIPS Int. Conf. (Cat. No. 01TH8569), IEEE, n.d. pp. 1926–1929 http://dx.doi.org/10.1109/NAFIPS.2001.944361.
[56] COVID-19: caso 32 | SIRM, 2020, https://www.sirm.org/2020/03/10/covid-19-caso-32/ (accessed April 23, 2020).
[57] False-color CT scan of normal heart & lungs images, 2020, https://www.google.com/url?sa=i&url=https%3A%2F%2Fwww.sciencesource.com%2Farchive%2FFalse-color-CT-scan-of-normal-heart---lungs-SS2302598.html&psig=AOvVaw38BDXDMrQewdLtl9YNlPdw&ust=1587731901192000&source=images&cd=vfe&ved=0CAIQjRxqFwoTCMjo-bjI_ugCFQAAAAA (accessed April 23, 2020).
[58] Normal brain (MRI) |RadiologyCase| Radiopaedia.org, 2020, https://radiopaedia.org/cases/normal-brain-mri-6 (accessed April 23, 2020).
[59] M.N. Wu, C.C. Lin, C.C. Chang, Brain tumor detection using color-based k-means clustering segmentation, in: Proc. - 3rd Int. Conf. Intell. Inf. Hiding Multimed. Signal Process. IIHMSP 2007, 2007, pp. 245–248, http://dx.doi.org/10.1109/IIHMSP.2007.4457697.
[60] COVID-19 pneumonia |RadiologyCase| Radiopaedia.org, 2020, https://radiopaedia.org/cases/covid-19-pneumonia-7 (accessed April 23, 2020).
[61] Lymph nodes on mammogram of the right breast |RadiologyCase| Radiopaedia.org, 2020, https://radiopaedia.org/cases/lymph-nodes-on-mammogram-of-the-right-breast?lang=us (accessed April 23, 2020).
[62] Normal pelvic ultrasound - transabdominal |RadiologyCase| Radiopaedia.org, 2020, https://radiopaedia.org/cases/normal-pelvic-ultrasound-transabdominal-1 (accessed April 23, 2020).
[63] N.K. Onteddu, Z. Hindi, G. Rajashekar, S.P. Kalva, Segmental arterial mediolysis presenting as spontaneous bilateral renal artery dissection, Radiol. Case Rep. 13 (2018) 495–498, http://dx.doi.org/10.1016/j.radcr.2017.11.017.
[64] Positron emission tomography |PsychologyWiki| fandom, 2020, https://psychology.wikia.org/wiki/Positron_emission_tomography (accessed April 23, 2020).
[65] Test images, 2020, https://homepages.cae.wisc.edu/~ece533/images/ (accessed August 14, 2020).
[66] M.A. Khanesar, E. Kayacan, M. Teshnehlab, O. Kaynak, Analysis of the noise reduction property of type-2 fuzzy logic systems using a novel type-2 membership function, IEEE Trans. Syst. Man, Cybern. B 41 (2011) 1395–1406, http://dx.doi.org/10.1109/TSMCB.2011.2148173.
[67] J. Li, C. Singh, Investigating and improving introductory physics students' understanding of the electric field and superposition principle, Eur. J. Phys. 38 (2017) 055702, http://dx.doi.org/10.1088/1361-6404/AA7618.

[68] D.L. Davies, D.W. Bouldin, A cluster separation measure, IEEE Trans. Pattern Anal. Mach. Intell. PAMI-1 (1979) 224–227, http://dx.doi.org/10.1109/TPAMI.1979.4766909.
[69] X.L. Xie, G. Beni, A validity measure for fuzzy clustering, IEEE Trans. Pattern Anal. Mach. Intell. 13 (1991) 841–847, http://dx.doi.org/10.1109/34.85677.
[70] J.C. Dunn, Well-separated clusters and optimal fuzzy partitions, J. Cybern. 4 (1974) 95–104, http://dx.doi.org/10.1080/01969727408546059.
[71] S.K. Pal, A. Ghosh, B.U. Shankar, Segmentation of remotely sensed images with fuzzy thresholding, and quantitative evaluation, Int. J. Remote Sens. 21 (2000) 2269–2300, http://dx.doi.org/10.1080/01431160050029567.